Fall 11-29-2010

BULGING FACTORS IN GEOMETRICALLY NONLINEAR CRACKED LAMINATED SHELL STRUCTURE UNDER DYNAMIC INTERNAL PRESSURE

Nitin B. Ingale Mr.
nitiningale@yahoo.com

BULGING FACTORS IN GEOMETRICALLY NONLINEAR CRACKED LAMINATED COMPOSITE SHELL STRUCTURE UNDER DYNAMIC INTERNAL PRESSURE

By

Nitin B. Ingale

A THESIS

Presented to the Faculty of

The Graduate College at the University of Nebraska

In Partial Fulfillment of Requirements

For the Degree of Master of Science

Major: Mechanical Engineering

Under the Supervision of Professor C. W. Solomon To

Lincoln, Nebraska

December, 2010

BULGING FACTORS IN GEOMETRICALLY NONLINEAR CRACKED LAMINATED COMPOSITE SHELL STRUCTURE UNDER DYNAMIC INTERNAL PRESSURE

Nitin B. Ingale, M.S.

University of Nebraska, 2010

Advisor: C. W. Solomon To

This thesis is about the investigation of the geometrically nonlinear responses and bulging factors of cracked laminated composite cylindrical shell structures subjected to internal pressure. Hybrid strain based three-node flat triangular shell elements, developed by To and Wang were used.

Effects of dynamic responses of various numbers of layers and their angle arrangements of cracked cylindrical shell structures clamped at both ends are analyzed and studied. Bulging factors based on the concept of equivalent Young's modulus of elasticity are found and compared with single and multiple layer composite cylindrical shell structures.

Finally, bulging factors for similar laminated composite cylindrical shells with free-free boundary conditions are also presented in this thesis.

Acknowledgements

I would like to take this opportunity to present my deep thanks to my advisor Dr. C.W. Solomon To, for his expertise, encouragement, continuous guidance and valuable time to time advice. This research would be impossible without his important guidance.

I would like to express my gratitude to Dr. K. P. Rajurkar from department of Industrial and Management Systems Engineering and Dr. W. M. Szydlowski from Department of Mechanical Engineering for being in my committee and reviewing my thesis.

I am thankful to Dr. To for letting me use the Fortran computer code developed by him and Dr. Bin Wang. The latter code was previously developed by Dr. Meilan Liu and Dr. To for analysis of isotropic shell structures.

I am also grateful to Jiming Fu for assistance in providing various input files, running of the Fortran computer code above, and continuous consultation via the internet.

My thanks also are for faculty and staff members of Mechanical Engineering Department at University of Nebraska Lincoln. Without support and encouragement of my friends, it would be tough to go through.

I would also like to be thankful to my brothers and friends.

Last but not least, I specially would like to be thankful to my father and mother, who gave me such a wonderful life and way to success.

Table of Contents

List of Figures

Chapter 1 Introduction

1.1 Background

Aircraft fuselage body undergoes pressurization and depressurization while it takes off and lands respectively. This cyclic variation in pressurization can cause stresses development over skin of fuselage of aircraft which may lead to crack existence. Crack developed is external crack and existence of crack may lead to catastrophic accident.

This chapter begins with a literature survey of existing work available and presentation of objectives of the present investigation. The final section is concerned with the organization of this thesis.

1.2 Geometrically Nonlinear Analysis of Laminated Composite Shell Structures

As composite materials offer tremendous advantages and the percentage of composite materials applied in aircrafts increases. Many studies have been performed. The development of reliable composite materials is one of the most important researches in the field of aircraft design and production. In this section shell structures without crack and undergoing large deformation modeled by the finite elements are reviewed.

Shear-flexible quadrilateral shell finite elements of 8 and 12-nodes developed by Noor and Mathers [1.1] were used for analyzing geometrically nonlinear behavior of

laminated shells. Triangular finite elements that have 6 nodes each [1.2] were developed and used for shear deformation of laminated shells. Reddy, Chang and Chao [1.3] also analyzed large and geometrically nonlinear deformation of shell structures with a doubly-curved shear-deformable shell element. Similar work were reported by Saigal, Kapania and Yang[1.4], Naidu and Sinha [1.5], and Rothert and Dehmel [1.6].

Lin, Farfad and Beaulieu [1.7] used a shell element for nonlinear analysis of composite bridges, in which small elasto-plastc strains and updated Lagrangian formulations were used for large displacement and rotation of the structures. Flat shell element based on free-formulation finite element concept was developed and geometrically nonlinear composite shell was analyzed for validation of the accuracy of new element by Madenci and Barut [1.8]. Zhu [1.9] analyzed sandwich and composite shells with the use of a curved triangular shell element. The latter can be used for linear and nonlinear in-plane shear behavior.

In the later part of 1990's, To and Wang [1.10] developed several hybrid strain or mixed formulation-based flat triangular composite shell finite elements to predict geometrically nonlinear responses of large deformed laminated composite plate and shell structures under transient excitations. The elements applied the incremental form of Hellinger-Reissner variational principle and updated Lagrangian description have advantageous features such as simplicity, elimination of shear locking, accuracy, efficiency, and capability of dealing with large deformation of finite strain and finite rotation. Two of these elements are rank sufficient and able to provide correctly the six rigid body modes.

1.3 Cracked Shell Structures and Bulging Factor

In parallel to the studies of laminated composite shell structures without crack, cracked shells were investigated by Folias [1.11-1.12] in 1965. He developed coupled singular integral equations for stress intensity factor λ for longitudinal cracks in pressurized shallow cylindrical shell. Later, Copley and Sanders [1.13] using linear thin shell theory obtained solutions for cylindrical shell with crack and internal pressure. They also investigated elastic behavior of a cracked cylindrical shell with the use of shallow shell theory and mentioned that their approach is sufficient for short cracks. Erdogan and Kibler [1.14] solved the integral equations and presented stress intensity factor λ values evaluated in the range of 0 to 8.

A popular measure and design parameter of isotropic cracked shell structures is the so-called bulging factor which has various definitions. Generally, the bulging factor is defined as the ratio of the stress intensity factor in a shell with a crack to the stress intensity factor in a flat plate of the same material, thickness, crack length and in-plane remote stress acting perpendicular to the crack line [1.15]. Cheryl, Young and Starnes [1.15] computed and compared bulging factors.

Ansell [1.16] reported that bulging factors involved with geometrically nonlinear deformation. Jeong and Tong [1.17], and Bakuckas *et. al.* [1.18] developed empirical equations for the bulging factor. Rose *et. al.* [1.19] discovered curvature induced coupling between the membrane making the local region around the crack to deform out of plane. They also showed that the bulging factor depends upon parameters, such as

shell geometry, loading condition. Rhaman *et. al.* [1.20] examined the effect of crack length, applied pressure and stiffening elements on bulging factors. They concluded that for longer cracks bulging factors vary nonlinearly with the presence of internal pressure.

Ayari *et al.* [1.21] had found out that by applying layer of plyisocyanurate (PIR) on inner side of the shell structure near the crack the bulging factor can be reduced by 45% depending upon shell configuration, foam thickness and internal pressure. They also concluded that bulging factor increases with increase in crack length but can be reduced efficiently with the application of foam layer.

Recently, Fu [1.22] has evaluated central deflections for multilayer cracked laminated composite shell structures under internal dynamic pressure. By applying the flat triangular shell finite elements developed by To and Wang [1.10], a relatively comprehensive examination was performed on the influences of crack types and crack lengths. He also investigated the bulging factors for single layer cylindrical shell structures with various boundary conditions.

1.4 Motivations and Objectives of Present Investigation

Due to the increased use of laminated composite shells in aerospace and ship building industries, a significant amount of efforts has been directed at the development of laminated composite shell finite elements over the years. Bulging factor is a measure established for cracked isotropic shell structures undergoing geometrically nonlinear

deformation. However, no measure similar to the bulging factor has been established for cracked laminated composite shell structures.

Therefore, the objectives of this research are (1) to investigate the dynamic responses of cracked multi-layer laminated composite cylindrical shell structures under internal pressure by applying the flat triangular laminated composite shell finite elements developed by To and Wang [1.10], and (2) to study and establish a measure similar to the bulging factor for cracked multi-layer laminated composite shell structures. To limit the scope of the present investigation only cylindrical laminated composite shell structures represented by the triangular finite elements will be considered.

1.5 Organization of Thesis

This thesis consists of 5 chapters and contents of the chapters are as mentioned below.

Chapter 1 gives an overview about the literature for previous work done and motivations as well as objectives for the research.

Chapter 2 deals with the development of the expression for bulging factor and information about the composite materials. A brief introduction to the hybrid strain or mixed formulation-based laminated composite triangular shell finite elements is also provided in this chapter.

Chapter 3 is concerned with finite element representation of the shell structures and it includes central deflections of multi-layer laminated composite shell structures with and without cracks.

Chapter 4 deals with the central deflections and bulging factors of cracked laminated composite cylindrical shell structures under different internal pressure.

Finally, Chapter 5 includes a summary, conclusion and recommendations for future research.

Chapter 2 Theoretical Development

2.1 Introduction

Aircrafts always carry high loads and are subjected to loading and unloading of passengers/goods, flight, landing and corrosion over period of time. Thus, fatigue cracks may develop. Presence of cracks can be dangerous over long span of time, as they may lead to dangerous accidents. Strengths of cracked areas are significantly weakened by stress cycles. Additionally the cracks can propagate under low and high cycles of stresses induced in the aforementioned loading environments.

To-date, a great percentage of aircraft bodies is made of composite materials for various reasons to be discussed in the following section. The mixed or hybrid formulation of the flat triangular shell finite elements to be applied in the present investigation is outlined in Section 2.3 while the empirical expressions for bulging factors of isotropic shell structures are briefly introduced in Section 2.4. An expression for bulging factor of laminated composite shell structures is presented in Section 2.5.

2.2 Composite Materials

A composite material is a combination of two or more distinct materials with a recognizable interface within them. For structural applications, the definition can be

revised to include those materials that consist of a reinforcing phase such as fibers or particles supported by a binder or matrix phase.

2.2.1 Advantages of composite materials

The main advantage of most composite materials is their light weight. A quick way to illustrate this advantage is in the strength to weight ratio. Different materials have different strengths. For a given design, the materials used must be strong enough to withstand the load that is to be applied. Usually this increases the bulk and weight of the parts. Another option is to change material to one that has high enough strength to begin with. The advantages of composite materials compared with metals in the aircraft construction are: longer lifecycle due to higher material fatigue resistance, corrosion resistance, easier maintenance, higher resistance to fire, easier material processing, possibility of designing more complex shapes, and lower specific weight of the material.

2.2.2 Applications of composite materials

Owing to the advantages of composite materials as mentioned in the last sub-section, demand is increasing with their usability. Use of composite materials in industries such as aviation, submarine, energy, automobile, bridge, military armors, and medical devices and so on has been common.

In particular, application of composite materials in aviation industries has been increased steadily. It is known that military aircraft has 75% of composite material while

and civilian has 60% [2.1]. The most commonly employed composite materials are carbon/epoxy, and graphite/titanium for aircraft wings and fuselages.

2.2.3 Different types of composite materials

Aside from natural composite materials, many man-made composite materials consist of two basic kinds. Weaker phase of material is called matrix which is reinforced by other strong and stiffer material. A layer between both of them is called the interphase layer. Classification of different types of composite materials is given in [2.2] (1) particulate which consists of particles of various shapes and sizes in a disperse manner; examples of particulate composite materials are concrete, glass; (2) discontinuous or short fiber composites which contain short fibers as reinforcing material and can be oriented in one direction or multi-directions; and (3) continuous fiber composites which are reinforced with long fibers such that they are more stiff and efficient. Continuous fiber composite materials can be mainly woven as multi-directional, such as cross-ply, angle-ply or unidirectional. Laminated composite consists of thin layers of different materials bonded together, like in bimetals and plywood. Figure 2.1 includes typical laminated composite materials [2.3-2.4].

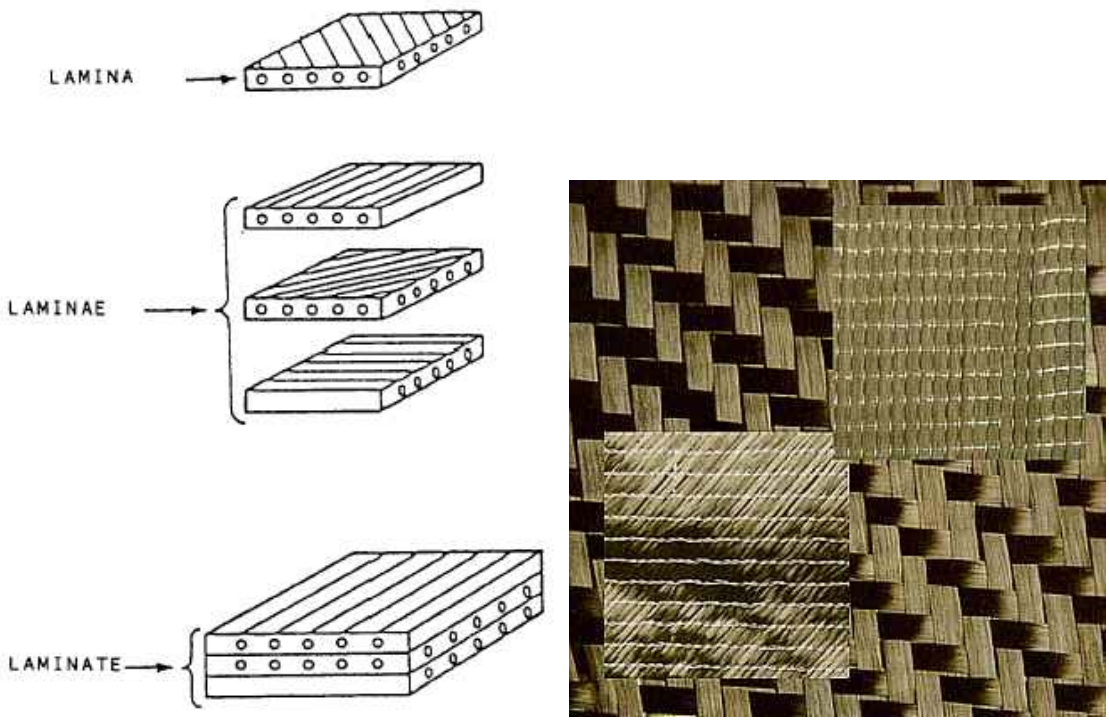

Figure 2.1 Laminated composite materials: (a) Unidirectional reinforcement, and (b) woven fabric reinforcement [2.3-2.4].

2.3 Mixed Formulation Based Three-node Flat Triangular Laminated Composite Shell Elements for Geometrically Nonlinear Dynamic Analysis

To and Wang [2.5, 2.6] have developed several flat triangular laminated composite shell elements based on the hybrid strain or mixed formulation for geometrically nonlinear dynamic analysis. Each of these elements has three nodes and every node has six degree of freedoms (dof). The latter include three translational and three rotational dof. These elements have several advantages such as being capable of dealing with large

deformation of finite strain and finite rotation, including the drilling dof (ddof), elimination of shear locking and ability to represent correctly the rigid body modes. The updated Lagrangian formulation and the incremental Hellinger-Reissner variational principle were employed to develop this element.

Because of their exclusive use in the present investigation and in order to provide a basic understanding of the steps involved in the formulation and derivation of element matrices an outlined is presented in the following sub-sections.

2.3.1 Incremental variational principle

The incremental variational principle employed is the Hellinger-Reissner functional given by [2.6] ,

$$\pi_{HR} = \int_V \left[(e^{\varepsilon})^{\mathrm{T}} C e^{u} - \frac{1}{2} (e^{\varepsilon})^{\mathrm{T}} C e^{\varepsilon} \right] \mathrm{dV} - \mathrm{W} \qquad (2.1)$$

where, e^{ε} is independently assumed strain field , e^{u} strain due to displacement; C is the elastic matrix; W is work done by external force, and the superscript $\boldsymbol{\varepsilon}$ and u indicate that the quantities are from independently assumed strain field and displacement field, respectively.

For geometrically nonlinear analysis with incremental formulation and updated Lagrangian description, the static and kinematic variables in current equilibrium configuration at time t are known quantities. The objective at this stage is to determine

their unknown values in the subsequent equilibrium configuration at time $t + \Delta t$. It can be shown that the incremental form of the Hellinger-Reissner functional is [2.6]

$$\Delta\pi_{HR} = \Delta\pi_{HR}(\Delta u, \Delta e^{\varepsilon}) = \int_V (I_1 + I_2)\, dV - \Delta W\,, \tag{2.2}$$

where $I_1 = (e^{\varepsilon})^T C(\Delta e^{u}) \quad + (\Delta e^{\varepsilon})^T C\ (\Delta e^{u})$,

$$I_2 = -\frac{1}{2}(\Delta e^{\varepsilon})^T C(\Delta e^{\varepsilon}) - (\Delta e^{\varepsilon})^T C(e^{\varepsilon} - e^{u})\,,$$

in which Δu is the vector of incremental displacement; Δe^{ε} is the vector of independently assumed incremental updated Green strains; Δe^{u} is the vector of incremental updated Green "geometric" strains or incremental Washizu strains; e^{ε} is the Almansi strain vector at time t which is accumulated from assumed incremental strains; e^{u} is the vector if Almansi strains at time t (due to displacement), and ΔW is the work-equivalent term corresponding to prescribed body forces and surface traction in configuration $C^{t+\Delta t}$. The second term on the right-hand side (RHS) of the integrand I_2 is the so-called compatibility-mismatch can be disregarded per reported by To and Wang [2.6]. Thus, equation (2.2) can be reduced to

$$\Delta\pi_{HR} = \int_V I_3 \mathrm{d}V - \Delta W \tag{2.3}$$

where $I_3 = -\frac{1}{2}(\Delta e^{\varepsilon})^T C(\Delta e^{\varepsilon}) + (\Delta e^{\varepsilon})^T C(\Delta \varepsilon^{u}) + \sigma^T(\Delta \varepsilon^{u}) + \sigma^T \Delta\eta^{u}$, $\sigma^T = (e^{\varepsilon})^{\mathrm{T}} C$ is the Cauchy (true) stress vector for the current configuration, and $\Delta\varepsilon^{u}$ and $\Delta\eta^{u}$ are the linear and nonlinear parts of the incremental Washizu strain vector, respectively.

2.3.2 Hybrid strain formulation

Equation (2.3) can be used to derive the element stiffness matrices for a hybrid strain based element. The strain field and displacement field assumed are

$$\Delta e^{\varepsilon} = P\Delta\alpha \ , \tag{2.4}$$

$$\Delta u = \phi\Delta q \tag{2.5}$$

where, P is strain distribution matrix, ϕ is the displacement shape function matrix, $\Delta\alpha$ is the vector of incremental strain parameters and Δq is the incremental nodal displacement vector.

Substituting equations (2.4) and (2.5) into (2.3) and after some algebraic manipulations, one can show that

$$H = \int_{V_e} P^T C P \ dV_e, \quad G = \int_{V_e} P^T C B_L \ dV_e,$$

$$k_{NL} = \int_{V_e} B_{NL}^T P B_{NL} \ dV_e, \quad F_1 = \int_{V_e} B_L^T \sigma \, dV_e, \tag{2.6}$$

$$k_L = \int_{V_e} G^T H^{-1} G \ dV_e,$$

$$(k_L + k_{NL})\Delta q = F(t + \Delta t) - F_1 \tag{2.7}$$

where F is the external nodal force vector in the neighbor configuration associated with the ΔW term in equation (2.3), B_L and B_{NL} are the linear and nonlinear strain-displacement matrices, while σ_C is the matrix containing the Cauchy stress components at

the current configuration, k_L is the element "linear" matrix, k_{NL} is the "nonlinear" or initial stress stiffness matrix and F_1 is the pseudo-force vector.

2.3.3 Nonlinear stiffness matrix

The derivation of the nonlinear element stiffness matrix involved various important steps and can be found in [2.6]. The crucial component in the derivation is the incremental displacements of an arbitrary point within the element. To proceed, one requires the consideration of an arbitrary point within an element in the local co-ordinate system as shown in Figure 2.2. This arbitrary point in the local co-ordinates is defined as

$$\begin{Bmatrix} r^t \\ s^t \\ t^t \end{Bmatrix} = \sum_{i=1}^{3} \xi_i \begin{Bmatrix} r_i^t \\ s_i^t \\ 0 \end{Bmatrix} + \boldsymbol{\zeta^t} \sum_{i=1}^{3} \xi_i V_i^t \tag{2.8}$$

where ξ_i is the natural or area co-ordinates, V_i^t denotes the director of node *i* at time *t* , and $\boldsymbol{\zeta^t}$ is the co-ordinate along the director direction and satisfies

$$\frac{-h^t}{2} \leq \zeta^t \leq \frac{h^t}{2}$$

with h^t representing the total thickness of the laminated composite shell at time *t*.

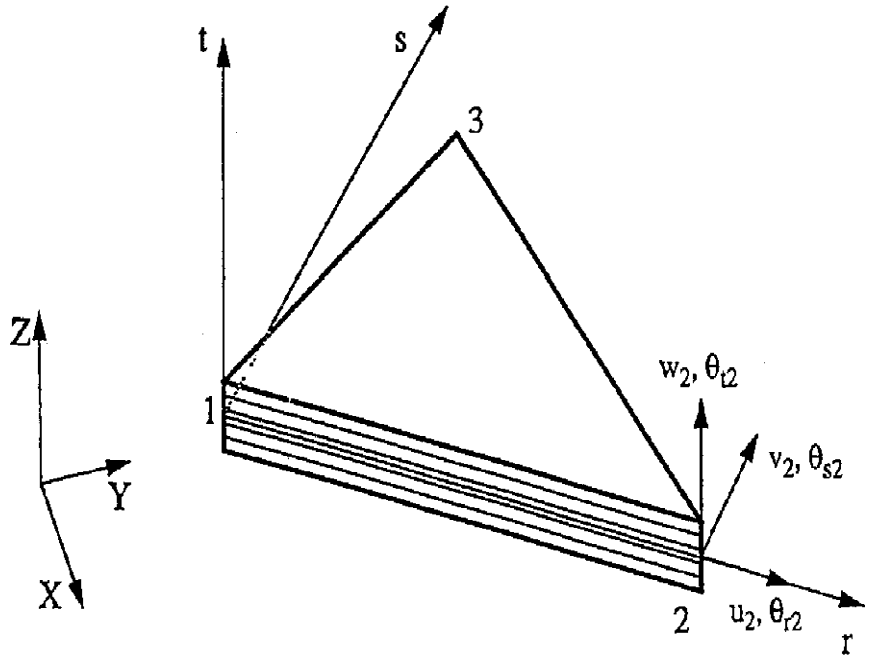

Figure 2.2 Flat triangular laminated composite shell element [2.6].

The incremental displacements of an arbitrary point within the element are therefore given as

$$\begin{Bmatrix} \Delta u^{\,t} \\ \Delta v^t \\ \Delta w^t \end{Bmatrix} = \sum_{i=1}^{3} \xi_i \begin{Bmatrix} \Delta u_i^t \\ \Delta v_i^t \\ \Delta w_i^t \end{Bmatrix} + \boldsymbol{\zeta^t} \sum_{i=1}^{3} \xi_i \, (\Delta V_i^t) \qquad (2.9)$$

Where, the first term on the RHS of equation (2.9) are the nodal incremental displacements of the element at the mid-surface of the element.

By employing the so-called exponential mapping, quadratic polynomials for the translational dof, incorporating the drilling dof (ddof), and after some lengthy algebraic manipulation, one can show that equation (2.9) reduces to

$$\begin{Bmatrix} \Delta u^{\,t} \\ \Delta v^{t} \\ \Delta w^{t} \end{Bmatrix} = \sum_{i=1}^{3} \xi_i \begin{Bmatrix} \Delta u_i^t \\ \Delta v_i^t \\ \Delta w_i^t \end{Bmatrix} + \Delta(\theta) \tag{2.10}$$

where

$$\square(\theta) = \boldsymbol{\zeta^t} \sum_{i=1}^{3} \xi_i \begin{bmatrix} \Lambda_{i(11)}^t & \Lambda_{i(12)}^t \\ \Lambda_{i(21)}^t & \Lambda_{i(22)}^t \\ \Lambda_{i(31)}^t & \Lambda_{i(32)}^t \end{bmatrix} \begin{Bmatrix} \Delta\theta^{\,t}_{ri} \\ \Delta\theta_{si}^t \end{Bmatrix} + \sum_{i=1}^{3} \begin{bmatrix} 0 & 0 & \overline{p}_i \\ 0 & 0 & \overline{q}_i \\ -\overline{p}_i & -\overline{q}_i & 0 \end{bmatrix} \begin{Bmatrix} \Delta\theta^{\,t}_{ri} \\ \Delta\theta_{si}^t \\ \Delta\theta_{ti}^t \end{Bmatrix}$$

and the remaining symbols have been defined in [2.6]. In the latter, equation (2.10) was used for the derivation of the incremental form of element linear stiffness matrix but it is not included here for brevity.

Apart from the derivation of the incremental form of element linear stiffness matrix the associated assumed incremental strain field is important. The assumed incremental strain field is in close analogy to the assumed strain field in linear analysis. It is defined as [2.6]

$$\Delta e^{\varepsilon} = \begin{Bmatrix} \Delta\varepsilon_m^{\varepsilon} \\ \Delta\gamma^{\varepsilon} \end{Bmatrix} + \boldsymbol{\zeta} \begin{Bmatrix} \Delta\chi^{\varepsilon} \\ 0 \end{Bmatrix} \tag{2.11}$$

where

$$\Delta\,\varepsilon_m^{\varepsilon} = P_m\,\Delta\alpha_m, \quad \Delta\chi^{\varepsilon} = P_b\,\Delta\alpha_b\,, \quad \Delta\gamma^{\varepsilon} = P_s\,\Delta\alpha_s\,, \tag{2.12}$$

$$\Delta\alpha_m = \{\Delta\alpha_1 \quad \Delta\alpha_2 \quad \Delta\alpha_3\}^T \quad , \tag{2.13a}$$

$$\Delta\alpha_b = \{\Delta\alpha_4 \quad \Delta\alpha_5 \quad \Delta\alpha_6\}^T \, , \quad \Delta\alpha_s = \{\Delta\alpha_7 \quad \Delta\alpha_8 \quad \Delta\alpha_9\}^T, \tag{2.13b,c}$$

in which the subscripts *m, b* and *s* denote the membrane, bending and transverse shear components of P in equation (2.4).

After some lengthy algebraic manipulations and applying the definitions

$$H_{mm} = \int_a P_m^T A' P_m da \, , \quad H_{sm} = \int_a P_s^T C_A^T P_m da \, ,$$

$$H_{ms} = \int_a P_m^T C_A P_s da \, , \quad H_{ss} = \int_a P_s^T E' P_s da \, ,$$

$$H_{bm} = \int_a P_b^T B' P_m da \, , \quad H_{bs} = \int_a P_b^T C_B^T P_s da \, ,$$

$$H_{mb} = \int_a P_m^T B' P_b da \, , \quad H_{sb} = \int_a P_s^T C_B^T P_b da \, ,$$

$$H_{bb} = \int_a P_b^T D' P_b da \tag{2.14}$$

and the matrix H in equation (2.6) becomes

$$H = \begin{bmatrix} H_{mm} & H_{mb} & H_{ms} \\ H_{bm} & H_{bb} & H_{bs} \\ H_{sm} & H_{sb} & H_{ss} \end{bmatrix}_{9\times 9} . \tag{2.15}$$

Similarly, matrix *G* in equation (2.6) can be found to be [2.6]

$$G = \begin{bmatrix} G_{mm} & G_{mb} & G_{ms} \\ G_{bm} & G_{bb} & G_{bs} \\ G_{sm} & G_{sb} & G_{ss} \end{bmatrix}_{9\times 18} \tag{2.16}$$

Therefore, with the component element stiffness matrix for the ddof k_{dd} included, and application of equation (2.7), the element stiffness matrix can simply be expressed as

$$k = k_L + k_{dd} + k_{NL}. \tag{2.17}$$

It should be noted that the orders of the matrices on the RHS of equation (2.17) are understood to be identical to that on the left-hand side (LHS) of equation (2.17).

2.3.4 Element mass matrix and loading vector

The derivation and definition of consistent element mass matrix and loading vector have been presented in [2.6] and they are not included in the present outline for brevity. However, on complement to equation (2.17), symbolically, the element consistent matrix is given by

$$m = m_t + m_r + m_d \tag{2.18}$$

in which m_t and m_r are the translational and rotational components of the consistent element mass matrix, respectively. Matrix m_d on the RHS of equation (2.18) is the part associated with the ddof.

2.4 Bulging Factors for Isotropic Shells

As mentioned in Chapter 1 one popular measure and design parameter of isotropic cracked shell structures is the so-called bulging factor which is defined as the ratio of the

stress intensity factor in a shell with a crack to the stress intensity factor in a flat plate of the same material, thickness, crack length and in-plane remote stress acting perpendicular to the crack line [2.7].

For a flat plate, the stress intensity factor is defined as [2.7]

$$K_p = \sigma_h \sqrt{\pi a}\, f(W) \tag{2.19}$$

where σ_h is the hoop stress, a is the half of crack length, and $f(W)$ is a function to account for finite width effects. The hoop stress σ for longitudinal cracks of shell structure is given as [2.7]

$$\sigma_h = p\frac{R}{h} \tag{2.20}$$

where p is the pressure inside the shell structure, R is radius of shell and h is thickness of the shell.

However, it has been pointed out by Ansell [2.8] that bulging involves with geometrically nonlinear deflection. Thus, the intensity factor is not a function of applied load. Therefore, a better approach is to include the effect of the intensity

$$K_s = \sqrt{\frac{E\gamma}{h}} \tag{2.21}$$

where γ is the strain-energy release rate, E is the Young's modulus.

By making use of equations (2.19) and (2.21), the bulging factor is then expressed in [2.7]

$$\beta = \frac{K_s}{K_p}. \tag{2.22}$$

Folias [2.9] presented the first analytical expression for the stress intensity factor in shells, which is only valid for small value of the shell parameter λ for isotropic shells. The shell parameter was given as

$$\lambda = \frac{a}{\sqrt{Rh}}[12(1-v^2)]^{1/4} \tag{2.23}$$

where v is Poisson's ratio, and the remaining symbols have already been defined in the foregoing.

The expression λ for larger values was provided by Erdogan and Kibler [2.10] using linear elastic fracture mechanics.

Chen and Schijve [2.11] presented another expression for the bulging factor as

$$\beta = \sqrt{1 + \left(\frac{5}{3\pi}\right)\left(\frac{Eha}{R^2p}\right)\left(\frac{0.316}{\sqrt{1+18\chi}}\right)\tanh\left(0.06\left(\frac{R}{h}\right)\sqrt{\frac{pa}{Eh}}\right)} \tag{2.24}$$

in which the ratio of the remote axial stress to the remote hoop stress, $\chi = \sigma_a/\sigma_h$ is present. It is worth writting that equation (2.24) is in good agreement with the results presented by Riks and Ansell [2.12].

Jeong and Tong [2.13] presented yet another expression for the bulging factor,

$$\beta = \sqrt{1 + 0.671\left[\left(\frac{E}{\sigma_h}\right)\left(\frac{a}{R}\right)\right]^{2/3}} \tag{2.25}$$

which was based on residual strength tests of curved panels with value of *a/R* ranged from 0.06 to 0.10.

Bakuckas *et al*. [2.14] established an equation for the bulging factor using results from a parametric nonlinear geometrical finite element study as

$$\beta = 1 + 0.775\left(\frac{E}{\sigma_h}\right)^{1/3}\left(\frac{a}{R}\right)^{5/6}. \tag{2.26}$$

In this equation the ratio of *a/R* was between 0.017 and 0.18, and hoop stress level ranged from 3.43 $\times 10^7$ Pa (5.0 ksi) to 1.37 $\times 10^8$ Pa (20.0 ksi).

2.5 Bulging Factors for Laminated Composite Shell Structures

Bulging factor equations developed so far, are useful for cracked isotropic shell structures. However, bulging factor equation for cracked laminated composite shell structures subjected to internal pressure is currently not available in the open literature. Consequently, To [2.15] suggested to an expression for such a bulging factor applied to cracked laminated composite shell structures. It is based on applying the bulging factor equation for isotropic shell structure in which now the Young's modulus of elasticity of the isotropic shell is replaced by the equivalent Young's modulus of elasticity of the laminated composite shell structure.

Specifically, it is known that the first natural frequency f_n of the isotropic shell structure is proportional to the square root of the Young's modulus of

$$f_n = \gamma \sqrt{E} \tag{2.27}$$

Where, γ is the proportionality constant and E is Young's modulus of the material of the isotropic shell structure.

Similarly, the first natural frequency of the multi-layer laminated composite shell structure, f_n^m is proportional to the square root of the equivalent Young's modulus, E^e such that [2.15]

$$E^e = \left(\frac{f_n^m}{f_n}\right)^2 E\,. \tag{2.28}$$

In other words, by determining the first natural frequencies of the cracked isotropic shell structure and the cracked multi-layer laminated composite shell structure one can obtain the equivalent Young's modulus of the laminated composite shell structure since the Young's modulus of the isotropic shell is given. The equivalent Young's modulus obtained by applying equation (2.28) can then be substituted into either equation (2.24) or (2.25) or (2.26) for the computation of the bulging factor of cracked laminated composite shell structure.

Chapter 3 Nonlinear Dynamic Responses of Cylindrical Shell Structures Without and With Crack

3.1 Cylindrical Shell

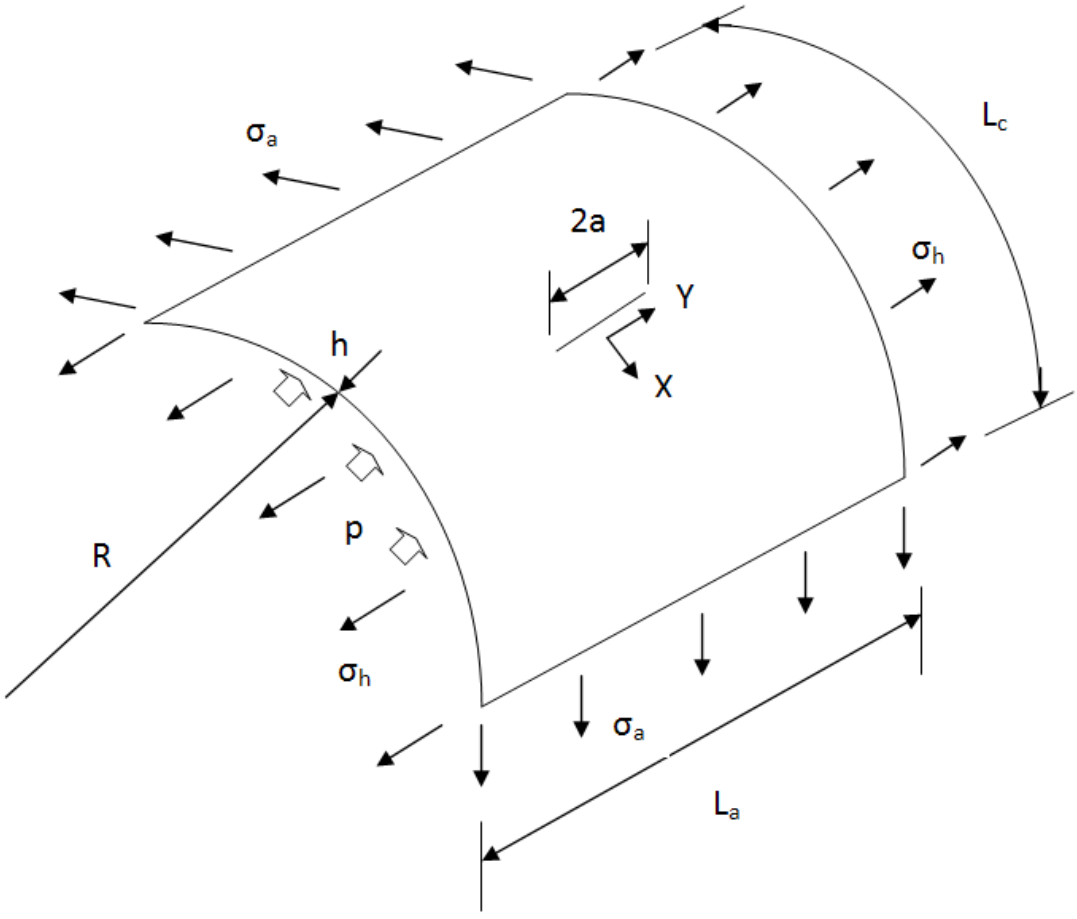

Figure 3.1 Cylindrical shell [3.1].

Cylindrical shell geometry shown in Figure 3.1 is studied and analyzed for the series of computational experiments. The shell structure presented in Figure 3.1 is one eighth segment of the whole cylindrical shell structure which was considered by Fu [3.1]. This chapter presents about dynamic responses of shell structures without and with crack. The shell shown in Figure 3.1 has a radius R, an axial length, L_a, a circumferential length, L_c, a wall thickness, h, and a crack length, 2a. The crack orientation is either longitudinal (parallel to the global Y-axis) or circumferential (parallel to the global X-axis). The shell is under internal pressure of p, which induces the internal stress $\boldsymbol{\sigma}_h$, and axial stress, $\boldsymbol{\sigma}_a$.

3.2 Laminated Cylindrical Shell Structure by Finite Element Approach

Hybrid laminated composite triangular shell elements (HLCTS) were used to analyze laminated composite shell structures by To and Wang [3.2] and resulted in finding out characteristics of HLCTS which are reflecting in dynamic responses of laminated composite structures. Every of the HLCTS having three nodes and each nodes has six degrees of freedom (dof) [3.1]. The latter include three translational and three rotational dof. The HLCTS are simple, capable of dealing with large deformation of finite strain and finite rotation.They include the so-called drilling degree of freedom (ddof), and are free of shear locking.

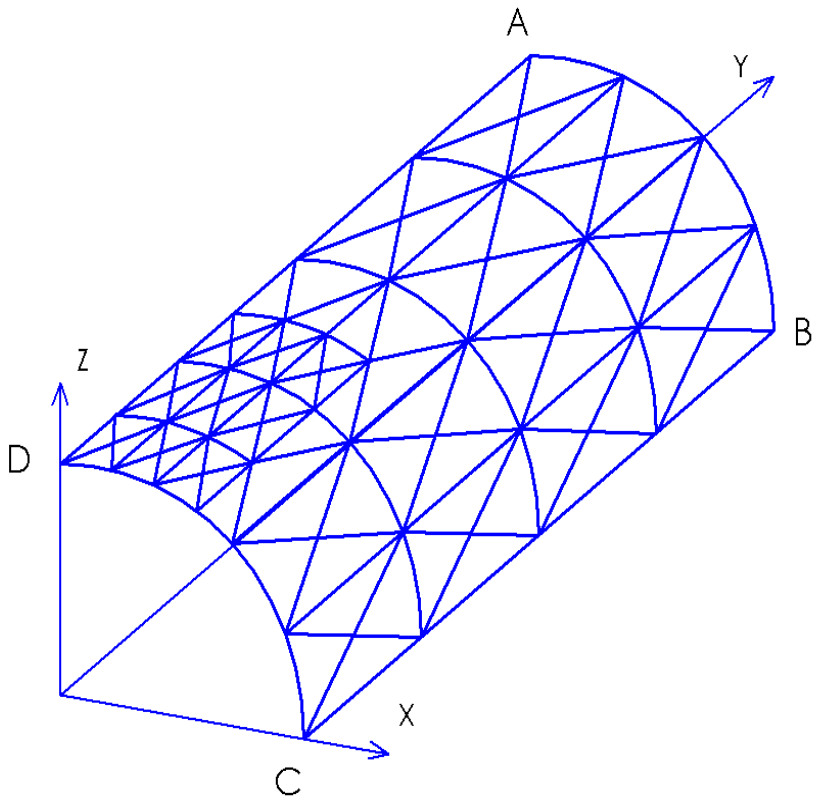

Figure 3.2 Laminated cylindrical shell structure with finite element representation [3.1].

Response of cylindrical composite shell structure was analysed with the use of typical model by using the finite element model as shown in Figure 3.2. Crack is present along the edge of AD in Figure 3.2. Area, where crack is present, is modified and refined with fine mesh to get more accurate result. Nodes of upper layer and nodes of lower layer have one to one correspondence within each other, which means, a similar mesh pattern is on both sides of the cylindrical laminated composite shell.

3.3 Finite Element Models of Laminated Cylindrical Panels without Crack and under Internal Pressure

First part of this section discusses about two layers composite shell structure for validating results previously derived. Secondly, this section talks about the multilayer cylindrical shell structure displacement. And next, cylindrical panel deflection with the different ply angles and how they vary with the different ply angles with comparison.

3.3.1 Two layers laminated composite cylindrical panel

In order to provide the foundation of the present investigation, in this section, previous results provided by To and Wang are validated [3.2] and discussion by Fu [3.1] in his dissertation are reproduced for the two layers cylindrical panel.

The specifications of the cylindrical panel are as mentioned below:

Cylindrical radius, R= 2.54 m,

arc length, L_c = 0.508m,

length, L_a= 0.508m, and

total thickness, h= 0.00127m.

Graphite-epoxy material was used for the cylindrical laminated composite shell structure and material properties are as mentioned below:

$E_1 = 1.3790 \times 10^{11}$ N/m^2 (2.0×10^7 psi),

$E_2 = 9.8599 \times 10^9$ N/m^2 (1.43×10^6 psi),

$G_{12} = G_{13} = G_{23} = 5.2402 \times 10^9$ N/m^2 (0.76×10^6 psi),

Poisson's ratio= 0.3, and

density $\rho = 1562.2$ kg/m^3 (5.644×10^{-2} lb/in^3).

Since, cylindrical panel is studied here, only one eighth of whole cylindrical panel is applied due to geometrical symmetry. The boundary conditions imposed on the whole shell structure are clamped on all sides of the panel. Thus, applied boundary conditions to the one eighth panel are: $V=\Theta_x= \Theta_y= \Theta_z= 0.0$, at CD, $U =\Theta_x= \Theta_y= \Theta_z=0.0$ at AD due to the symmetry boundary conditions imposed side AB and BC have a clamped boundary condition. Shear correction factors and step applied internal pressure to cylindrical panels are $k_4= k_5=(5/6)^{1/2}$ and p = 6895.0 N/m^2 (1.0 psi).

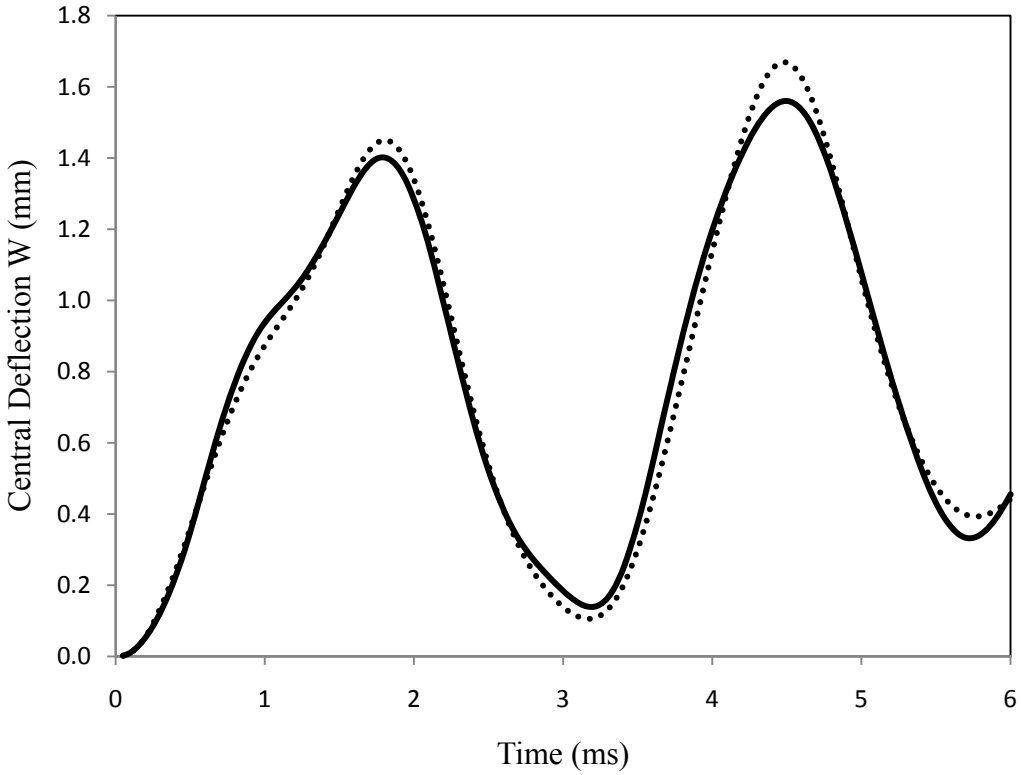

Figure 3.3 Response of the two layer cylindrical shell:

-, Present result; •, Ref. [3.1].

Figure 3.3 shows the transient response of the cylindrical shell structure along Z direction with ply angle [0/90] at point D shown in Figure 3.2. In Figure 3.3, results are reproduced which confirms the those obtained by To and Wang [3.2]. Trapezoidal integration scheme is applied with the time step 0.05 ms.

It is observed that the present results are identical to those of To and Wang [3.2] which agree very well with those obtained by Wu and Yang [3.3]. This confirmation check was used as a basis for continuous research with the FEM model and mesh.

3.3.2 Four layers laminated composite cylindrical panel

As shown earlier results in Figure 3.3, same trapezoidal integration scheme with HLCTS^{qd} elements were used for evaluating transient response of four layer panel without crack. Geometrical specifications and boundary conditions were kept the same as the two layer laminated cylindrical panel. The ply angles within four layers are restricted to $[0/45]_{sym}$ for results shown in Fig 3.4.

Figure 3.4 shows the transient response of four layer cylindrical composite shell structure and these results are similar to those obtained by To and Wang [3.2], which shows central deflection with the presence of internal pressure.

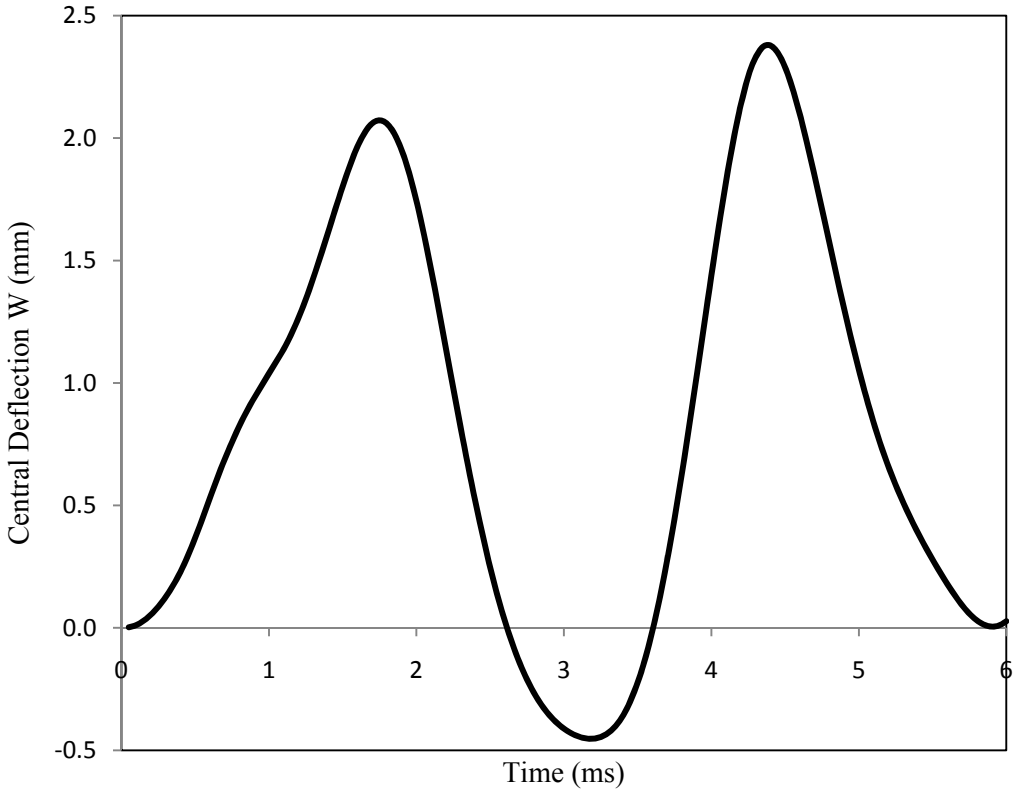

Figure 3.4 Response of the four layer cylindrical shell.

3.3.3 Eight layers laminated composite cylindrical panel

Figure 3.5 shows the transient response of central deflection of eight layer composite shell structure with the clamped boundary conditions on all sides with the similar physical dimensions of cylindrical shell and material properties as used for the two and four layer studies presented in the foregoing. The ply angles for the eight layers were maintained $[0/45/45/0]_{sym.}$

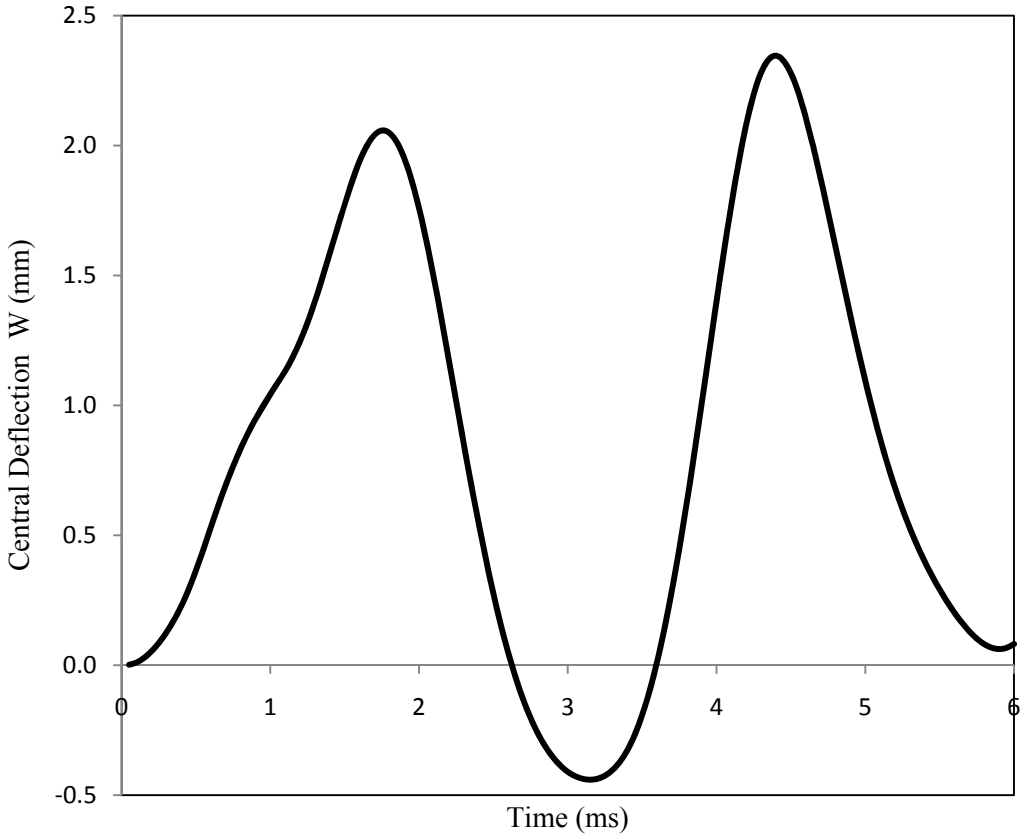

Figure 3.5 Response of the eight layer cylindrical shell

3.3.4 Comparison of various ply angles arrangements for two layer case

Transient response of two layer composite shell varies as ply angle varies, which is seen in the Figure 3.6. In this case, all parameters are kept identical to those considered previously but only ply angles are varied. Angle for first layer is kept at 30 degree for all the cases and ply angle between two layers are varied.

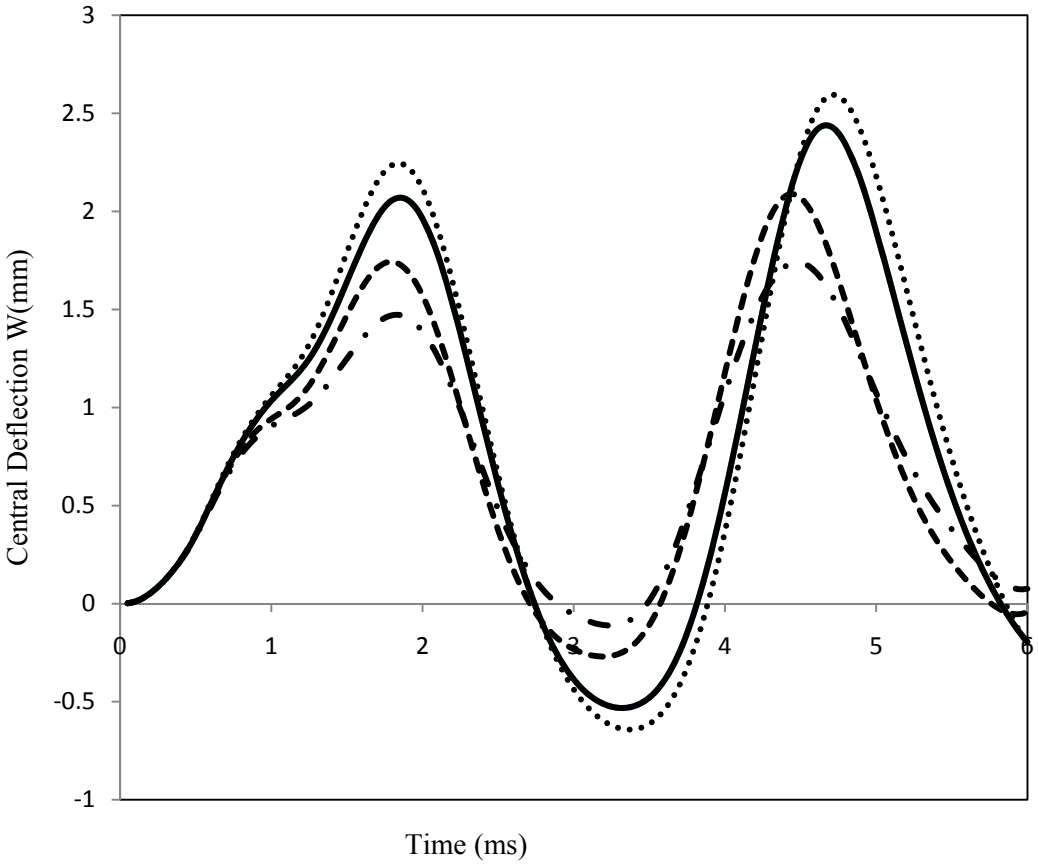

Figure 3.6 Responses of two layers with first angle constant:

– –, [30/0]; . . . , [30/45]; –, [30/60]; – . – .. , [30/90].

Figure 3.6 shows keeping one layer angle constant and varying another angle of ply, however Figure 3.7 shows the displacement with varying both ply angles between two layers. It can be easily determined that response of cylindrical shell displacement varies with ply angles within laminas. As shown in Fig 3.7, the case of ply angle (30,90) has maximum displacement of 1.75 mm whereas that for ply angle (30,45) shows 2.5mm.

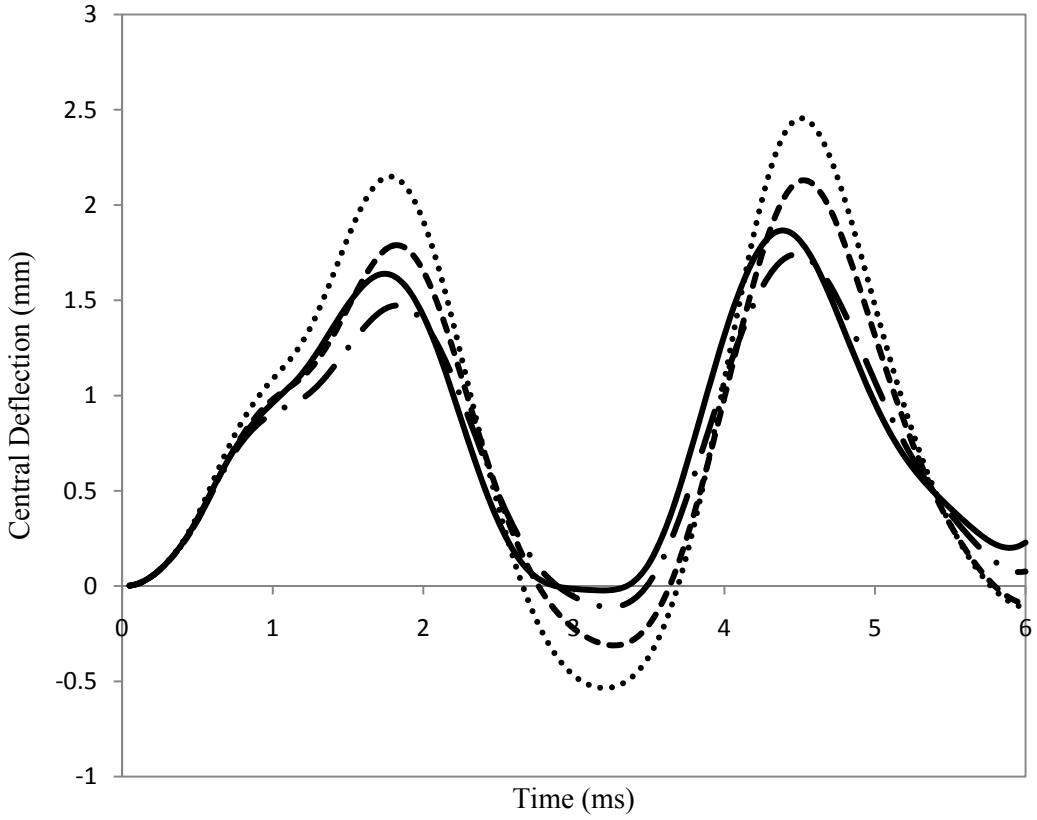

Figure 3.7 Responses of two layers with different ply angles:

– –, [15/60]; – . – ., [30/90]; . . , [45/15]; –, [90/30].

3.3.5 Comparison of various ply angles arrangements for four layer case

Keeping all boundary conditions and geometrical parameters identical to those studied in the foregoing, the four layer laminated composite shell structure was tested under presence of internal pressure and its displacements were recorded as shown in Figure 3.8. Significant changes in displacement can be seen with changing ply angles. It can be noticed that maximum displacement for the case with $[0/30]_{sym}$ is 1.75mm, whereas 2.25mm is for that with $[30/60]_{sym}$ condition.

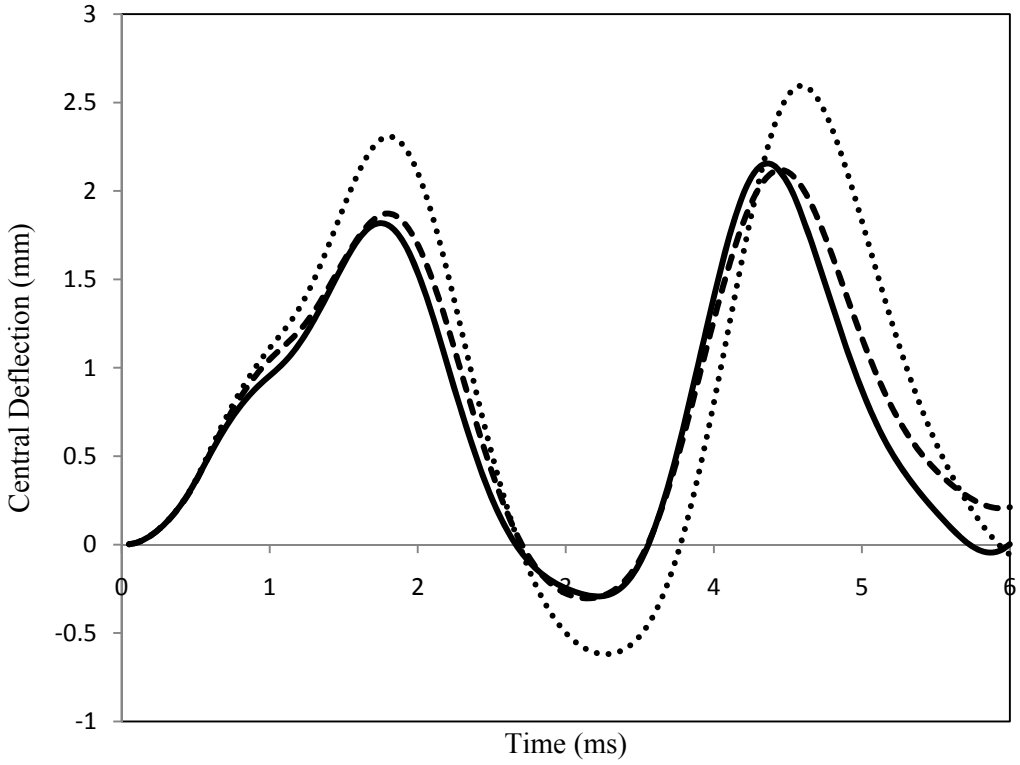

Figure 3.8 Responses of four layers with different ply angles:

– , $[0/30]_{sym}$; • • , $[30/60]_{sym}$; – – , $[45/90]_{sym.}$

3.4 Finite Element Models of Cracked Laminated Composite Cylindrical Panels under Internal Pressure

This section is concerned with the studied of the central deflection of the crack behavior with the presence of internal pressure. Discussion is made first for single layer and then multilayer cases for better understanding. Geometrical parameters are as mentioned below:

radius of cylindrical shell = 1.98m,

skin thickness = 1 mm,

composite material used = carbon/epoxy (AS4/3501-6),

$E=1.47\times10^{11}$ N/m^2 (2.13×10^7psi),

Poission's ratio $\upsilon_{12} = 0.27$, and density $\rho = 1600.0$kg/m^3 (5.8×10^{-2} lb/in^3).

The cylindrical shell considered, is the same as that used for the results without crack presented above.

It may be appropriate to note that in the numerical experiments computed results based on the time step size of $\Delta t = 0.01$ ms were found to be very close to those with $\Delta t = 0.005$ ms. Hence, in order to save computational time, all computational experiments were conducted $\Delta t = 0.01$ ms.

3.4.1 One layer cracked laminated composite cylindrical panel

In order to study the multilayer laminated composite shell structures, the one layer model for every case is considered first so as to provide a basis of reference to the multilayer results. This single layer case has been studied by Fu [3.1].

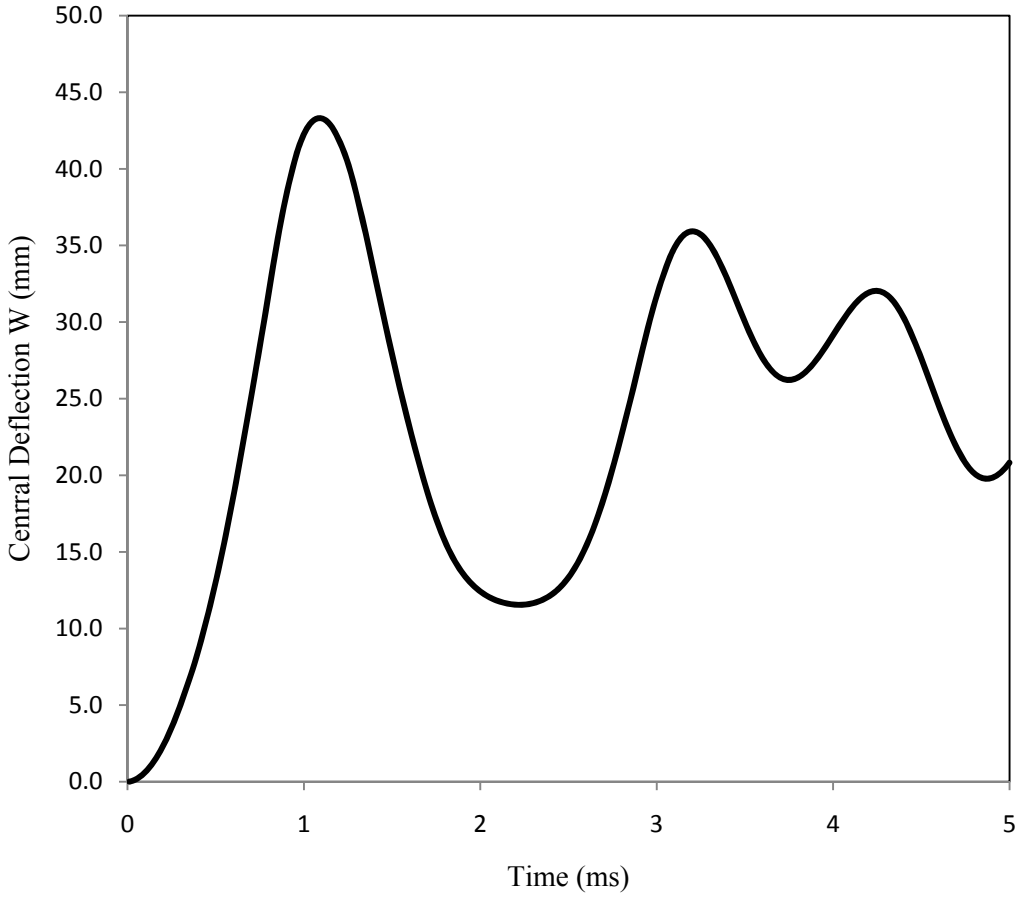

Figure 3.9 Response of the one layer cylindrical shell with crack.

Crack is present in longitudinal direction to the cylindrical shell, where ratio of two times crack length to the whole length of cylinder ($2a/L_a$) and ratio of crack width to crack length, b/a considered to be 0.375 and 0.1 respectively. It is noted that the computed results are identical to those presented in [3.1]. For this case, the first natural frequency was found to be 2227 rad/s which is identical to that found by Fu [3.1].

3.4.2 Two layers cracked laminated composite cylindrical panel

Geometrical shape and boundary conditions are kept constant as those mentioned in Sub-section 3.4.1. However, internal pressure used is limited to 101,325 Pa (14.7 psi) and material used for cylindrical shell was Carbon/Epoxy (AS4/3501-6). Thus, the material properties are:

$E_1=1.47\times10^{11}$ N/m^2 (2.13×10^7psi),

$E_2=10.3\times10^9$ N/m^2 (1.50×10^6psi),

$G_{12}= G_{13}= G_{23}=7.0\times10^9$ N/m^2 (1.0×10^6psi),

Poission's ratio $\upsilon_{12} = 0.27$, and

density $\rho = 1600.0$kg/m^3 (5.8×10^{-2} lb/in^3).

Figure 3.10 shows the central deflection of the two layer cracked shell structure with ply angle between the composite materials being 0 and 45^o.

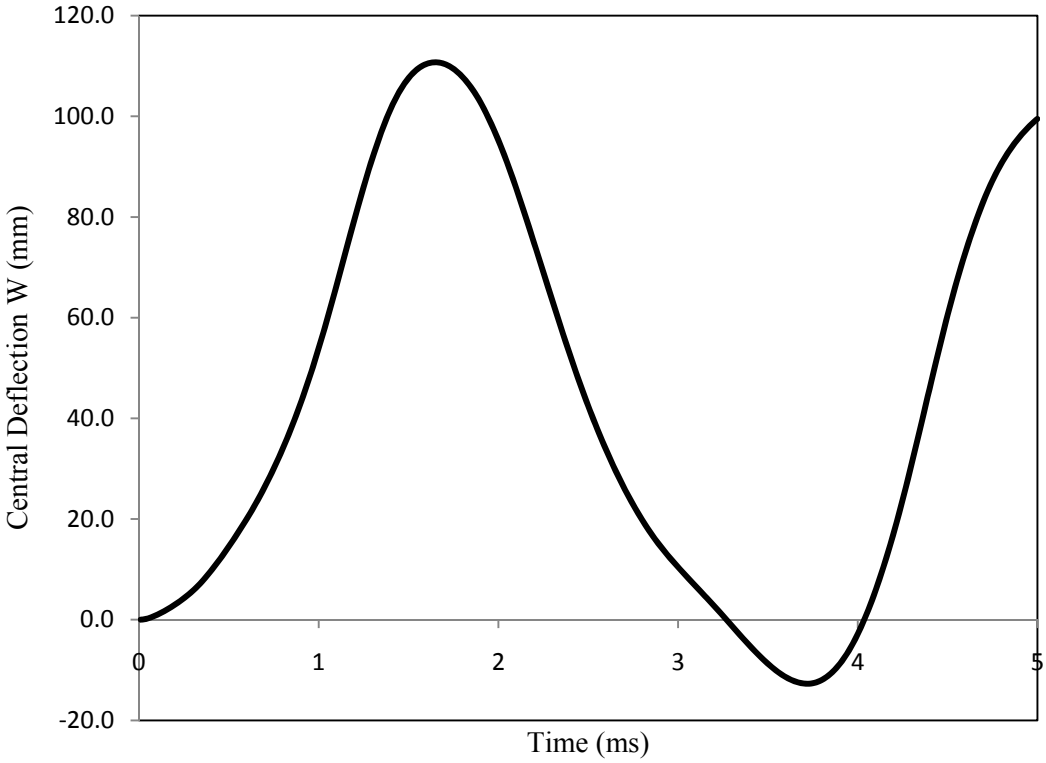

Figure 3.10 Response of the two layer cylindrical shell with crack.

Figures 3.11 and 3.12 shows result for the central deflection of the cracked shell structure with different ply angle arrangements and under internal pressure. Clearly, with different ply angles the central deflections are very much different. In Figure 3.11 it seems that the larger the difference of the angle between the plies the more stiff the structure becomes since the central deflection is reduced. Specifically, in Figure 3.11 the [0/90] case is the most stiff one.

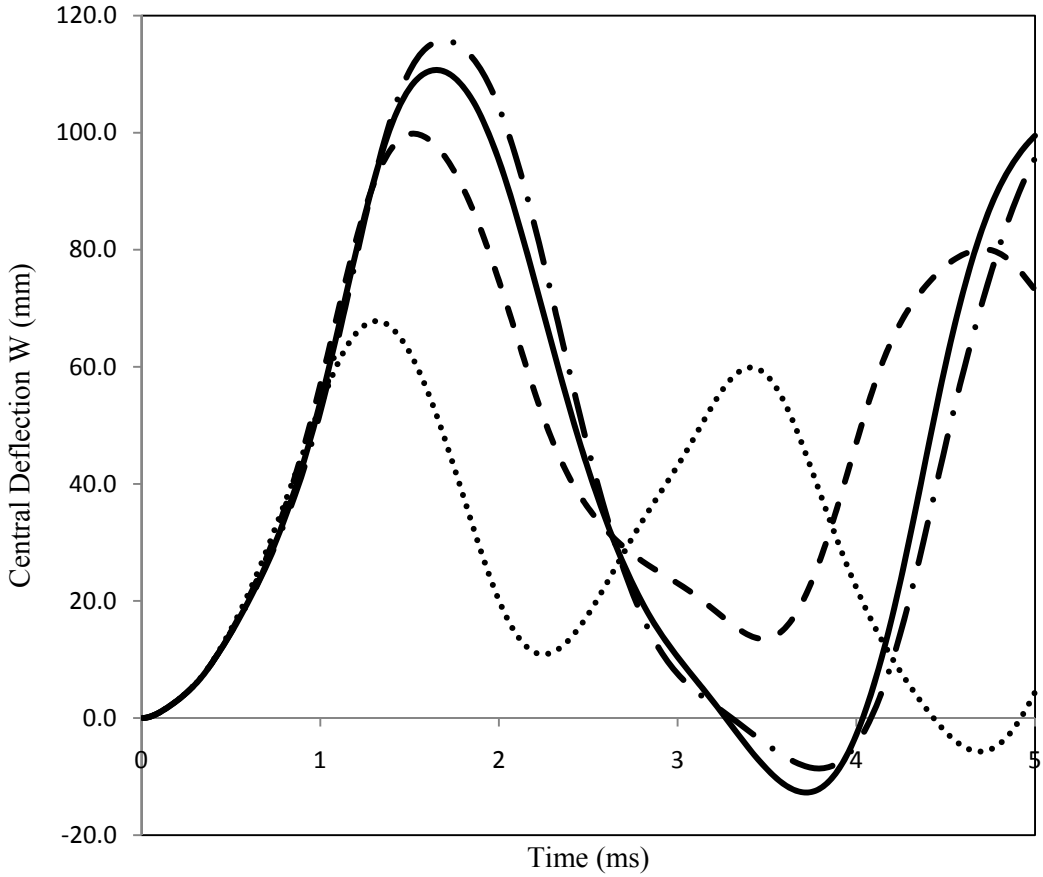

Figure 3.11 Responses of two layer cylindrical shell with crack:

- . - .,[0/30]; - , [0/45]; - -, [0/60]; . . . ,[0/90].

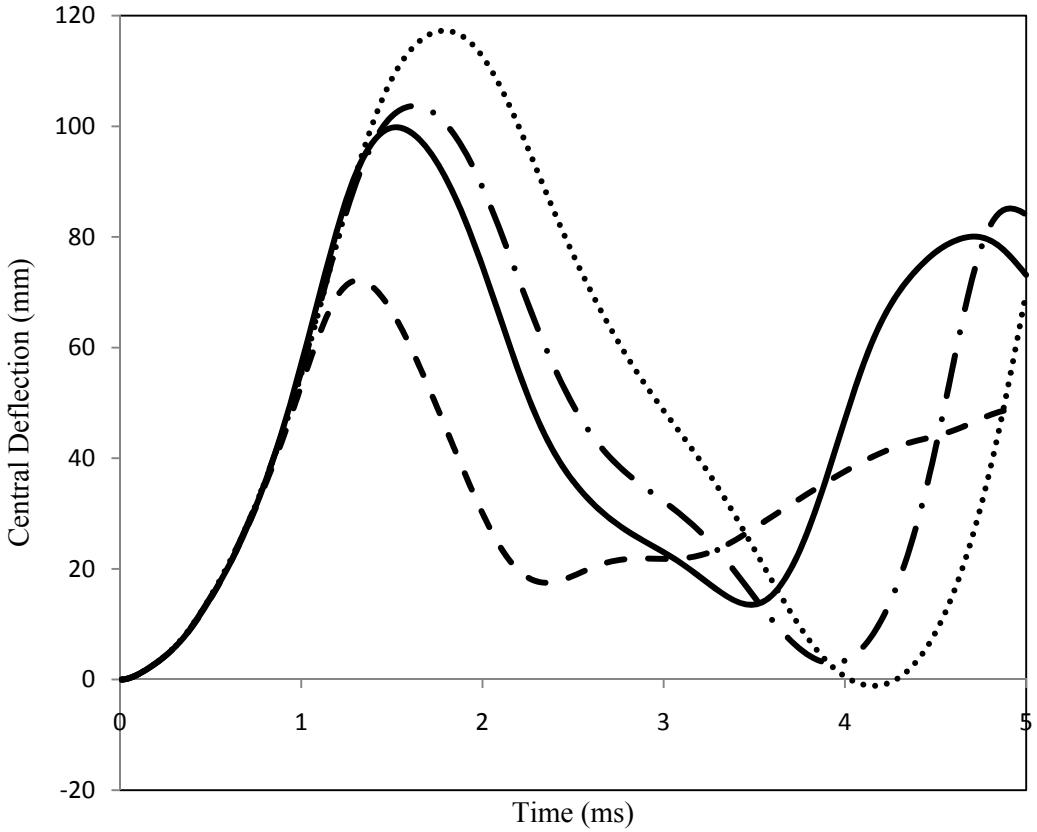

Figure 3.12 Responses of two layer cylindrical shell with crack:

-, [0/60]; - - , [30/45]; . . , [60/30]; - . - . , [90/60].

3.4.3 Four layer cracked laminated composite cylindrical panel

This is the case with ply arrangement as $[45/60]_{sym}$. All boundary conditions, geometric parameters and loading conditions are similar to those in the previous section. It can be noticed that total thickness of the shell structure is kept constant irrespective of the layers.

The material properties are:

$E_1 = 1.47\times10^{11}$ N/m^2 (2.13×10^7psi),

$E_2 = 10.3\times10^9$ N/m^2 (1.50×10^6psi),

$G_{12} = G_{13} = G_{23} = 7.0\times10^9$ N/m^2 (1.0×10^6psi),

Poission's ratio $\upsilon_{12} = 0.27$, and

density $\rho = 1600.0$kg/m^3 (5.8×10^{-2} lb/in^3).

The crack length to axial length ratio is $2a/L_a = 0.375$ and ply angle arrangement considered is $[45/60]_{sym.}$

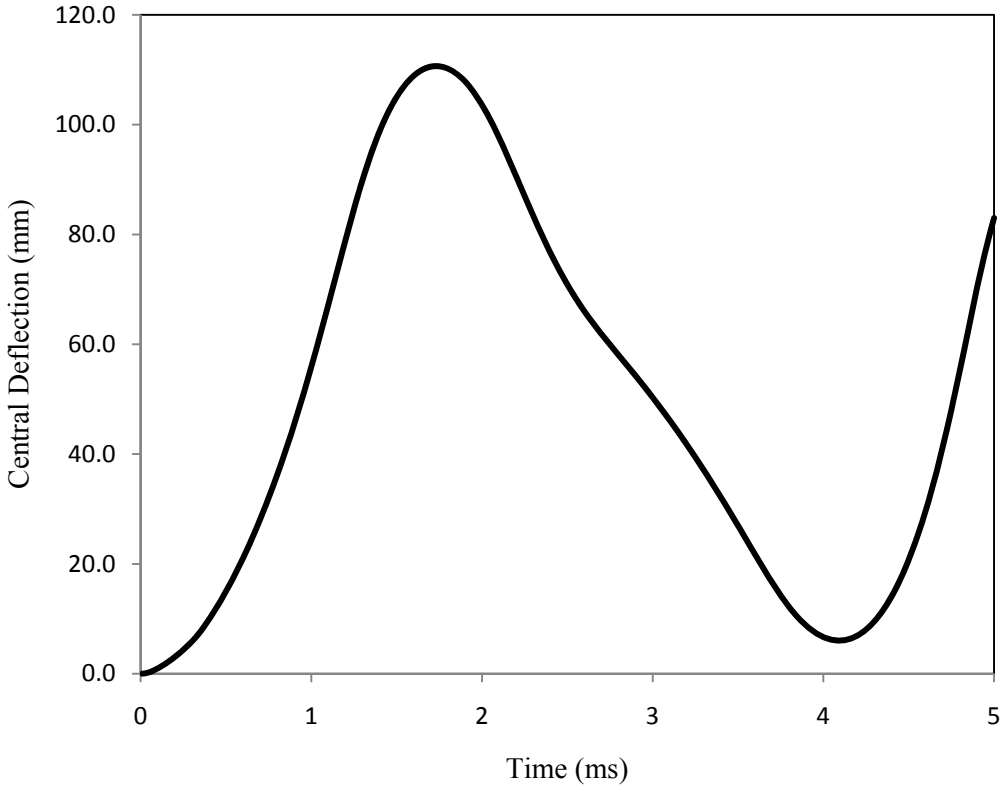

Figure 3.13 Response of four layer cylindrical shell with crack ply arrangement [45/60].

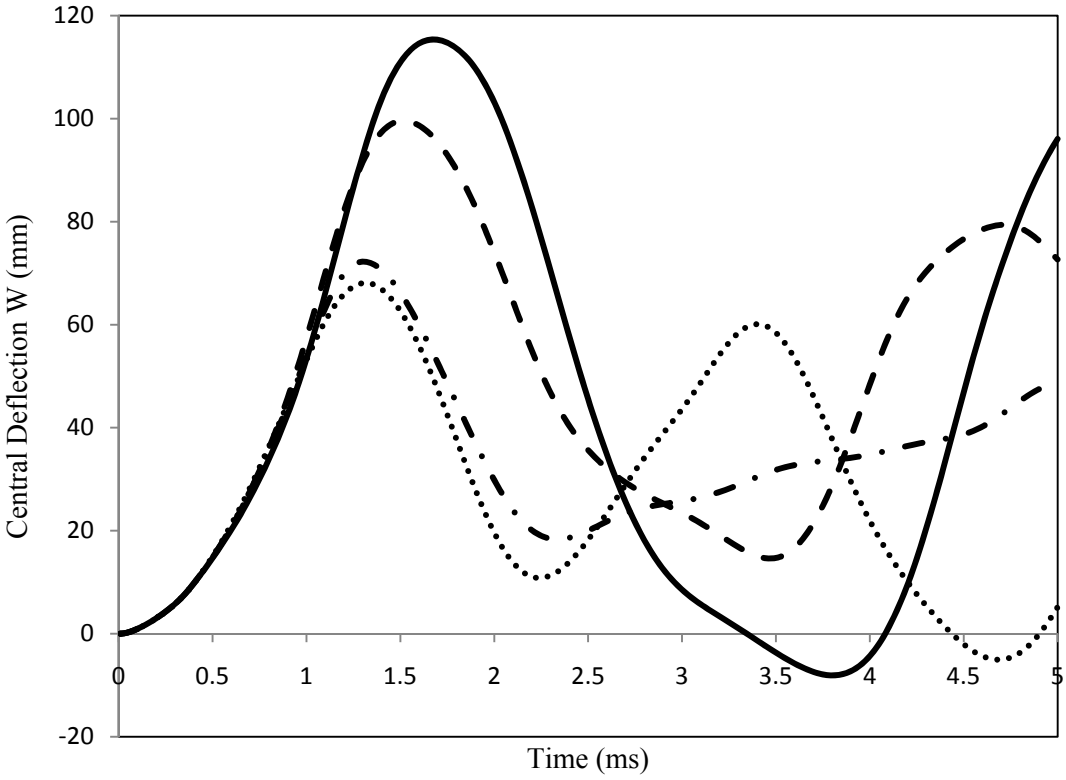

Figure 3.14 Responses of four layer cylindrical shell with crack:

-, $[0/30]_{sym}$; - - , $[0/45]_{sym}$; . . , $[0/60]_{sym}$; - . - . , $[0/90]_{sym}$.

Figure 3.13 shows results for the four layer laminated composite shell structure with ply angle arrangement of $[45/60]_{sym}$. Keeping geometrical parameters and other properties constant, but only changing ply angles within layers, results of various ply angle arrangements were plotted against time in Figures 3.14 and 3.15.

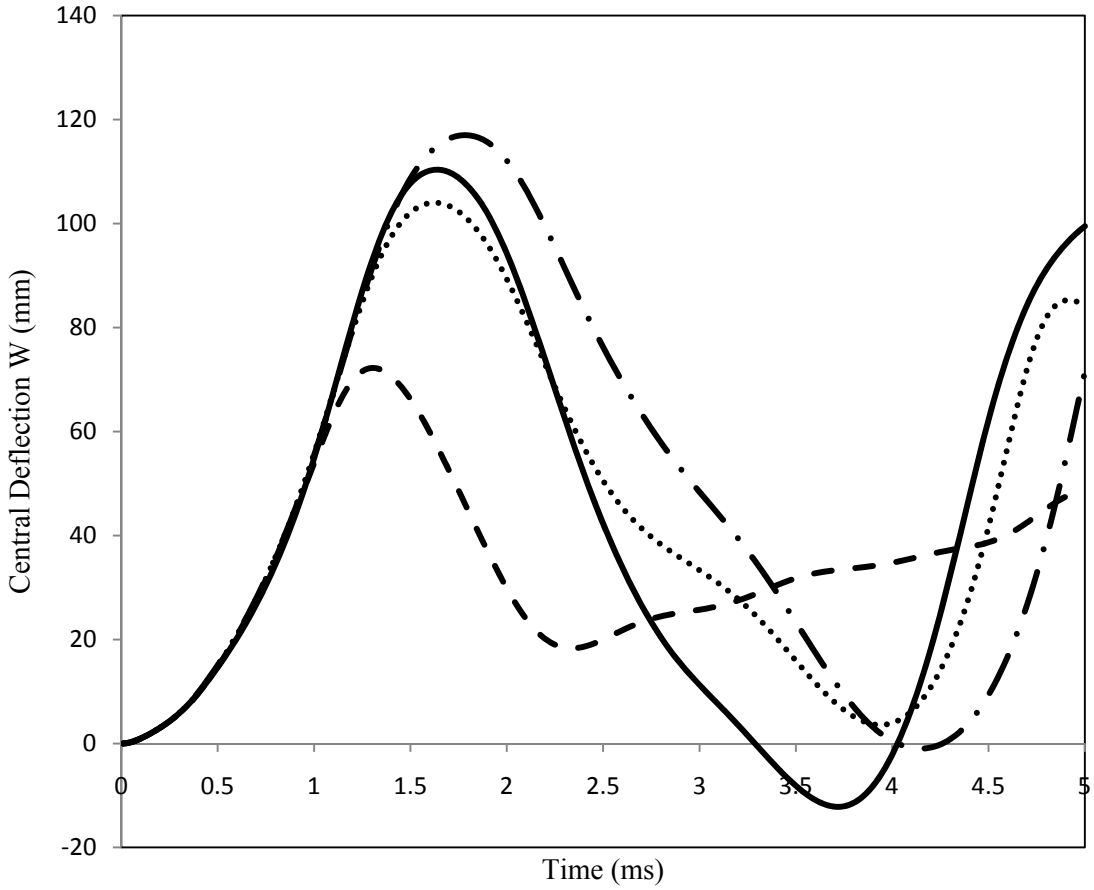

Figure 3.15 Responses of four layer cylindrical shell with crack:

– , $[0/45]_{sym}$; . . , $[30/60]_{sym}$; – . – . , $[45/30]_{sym}$; – – , $[90/60]_{sym}$.

Chapter 4 Bulging Factors for Shell Structures with Crack

4.1 Introduction

Bulging factors for cracked isotropic shell structures introduced in Chapter 2 where an approach for the determination of bulging factors for cracked laminated composite shell structures proposed by To [4.1] was also presented. To limit the scope of the investigation, in this chapter, only central deflections and bulging factors for laminated composite cylindrical shell structures are presented and discussed. Behaviors of cracked shell structures with respect to different internal pressures as well as different ply angles are shown. Internal pressure is varied and limited to the theoretical limit for atmosphere of 0.1013565 MPa (14.7 psi).

The computed results presented in this chapter, are concerned with the cylindrical shell structure representing Airbus A-320 [4.2] of radius 1.98m, length 8.00 m, and thickness 1.00 mm. This is the same shell structure investigated in [4.3]. The composite material used for the study was Carbon/Epoxy (AS4/3501-6). Two sets of boundary conditions are included in this chapter. The first set is identical to that mentioned in the last chapter and the finite element mesh adopted is that presented in Figure 3.2. That is, $V = \Theta_x = \Theta_z = 0.0$ at CD, $U = \Theta_y = \Theta_z = 0.0$ at AD, $W = \Theta_x = \Theta_y = 0.0$ at BC, and AB is fixed. The second set is that of free-free boundary conditions. The results for the first set of boundary conditions are included in Sections 4.2 through 4.5 while those for the

second set are presented in Section 4.6. The same time step size employed in Chapter 3, $\Delta t = 0.01$ms was employed in this chapter.

For completeness and direct comparison the next section deals with studies of an isotropic cracked cylindrical shell structure of the same geometrical dimensions given above. With reference to Figure 3.2, the longitudinal crack is along AD and located at the refined element region. Thus, the central deflection referred to in this chapter and and in Chapter 3 is at point D. That is, the central deflection is in the Z direction at point D which is at the mid-point of the crack.

4.2 Central Deflection and Bulging Factors for Single Layer Shell Structure

The single layer cylindrical shell structure studied in this section is that considered in [4.3]. Material properties of Carbon–epoxy (AS4/3501-6) for this shell structure are:

$E_1 = 1.47 \times 10^{11}$ N/m^2 (2.13×10^7 psi),

Poisson's ratio ν_{12}=0.27, and

density $\rho = 1600.0$ kg/m^3 (5.8×10^{-2} lb/in^3).

4.2.1 Central deflection for single layer cracked shell structure

The specific ratio of half crack length to radius of the shell structure considered in this sub-section is a/R = 0.1875. The computed results of the central deflection with internal pressures are presented in Figure 4.1 which is identical to that presented by Fu in [4.3]. It may be appropriate to note that all the deflections presented are those of the largest peak values at corresponding internal pressures. The first natural frequency for this case is 410.5 rad/s. It is seen that the central deflection increases with increasing internal pressure which is logical in the sense that as the internal pressure is increased the central point D of the crack becomes less stiff and therefore the deflection increases.

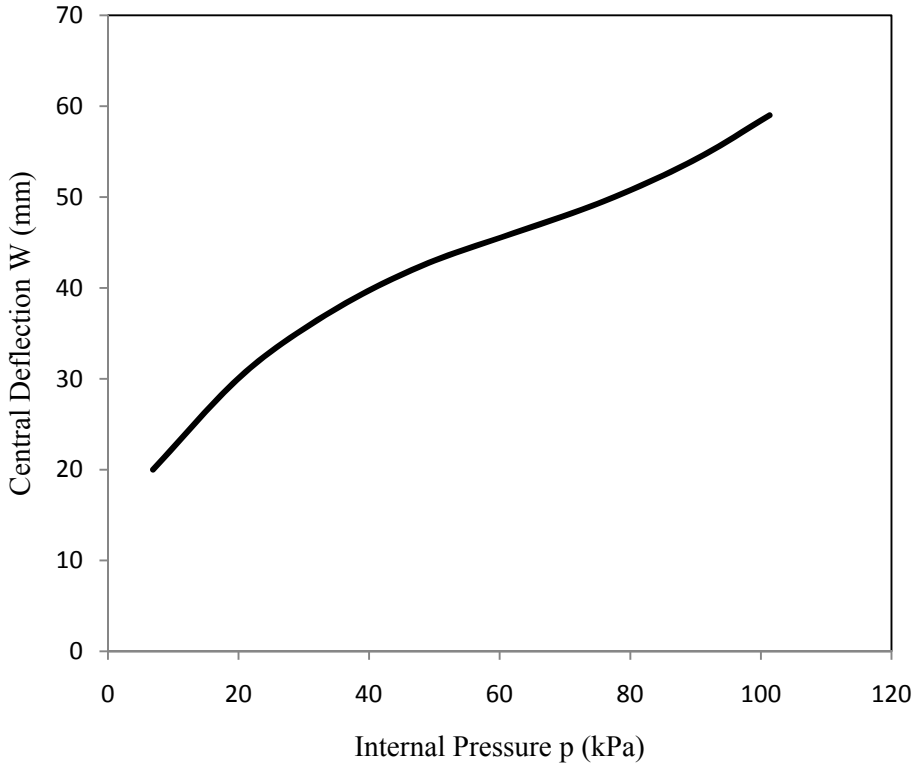

Figure 4.1 Central deflection for single layer shell.

4.2.2 Bulging factor for single layer shell structure

As mentioned Chapter 2, bulging factor for single layer shell structures is related to the stress intensity towards the crack tip and which is defined by equation (2.27) in Chapter 2. For a particular material the Young's modulus of elasticity remains constant, the bulging factor reduces with increasing hoop stress which is directly related to the internal pressure, as given by equation (2.27). This behavior is clearly shown in Figure 4.2. It is observed that the central deflection and bulging factor of the crack have opposite trends in the sense that the central deflection increases with increasing internal pressure while the bulging factor decreases with increasing internal pressure. This observation is similar to that provided in [4.3]. The explanation for the bulging factor is that since the bulging factor is approximately inversely proportional to the hoop stress of the shell structure as the internal pressure increases the hoop stress also increase so that the bulging decreases. The reason why the bulging factor decreases as the hoop stress increases can loosely be interpreted as the following. When the hoop stress increases the region of the surface around the crack is being pulled more intensely and in effect the bulge is being reduced.

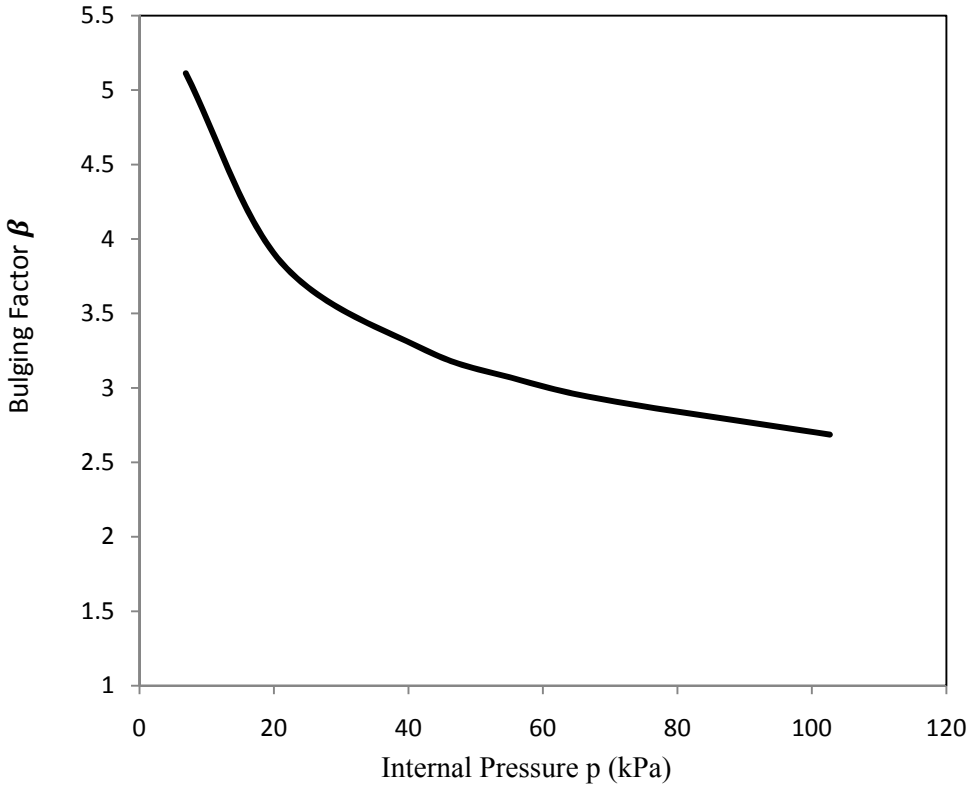

Figure 4.2 Bulging factor of single layer cylindrical shell.

4.3 Central Deflection and Bulging Factors for Two Layers Cylindrical Shell

This section is concerned with the central deflections and bulging factors with increasing internal pressure for two layer cracked cylindrical shell. The total thickness of the two equal layers is the same as the single layer case. This provides, loosely speaking, a basis for comparison to that of the single layer shell structure presented in the last section. Bulging factors of multi-layer shell structures equations (2.29 and 2.27) are employed for the computation.

Carbon–epoxy (AS4/3501-6) was used and its properties are:

$E_1 = 1.47 \times 10^{11}\ \text{N/m}^2\ (2.13 \times 10^7\ \text{psi})$,

$E_2 = 10.3 \times 10^9\ \text{N/m}^2\ (1.50 \times 10^6\ \text{psi})$,

$G_{12} = G_{13} = G_{23} = 0.7 \times 10^9\ \text{N/m}^2\ (1.0 \times 10^6\ \text{psi})$,

Poisson's ratio $\nu_{12} = 0.27$, and

density $\rho = 1600.0\ \text{kg/m}^3\ (5.8 \times 10^{-2}\ \text{lb/in}^3)$

4.3.1 Central deflection

Figure 4.3 shows the variation of central deflections with internal pressure for the [0/30] case. The behavior is similar to that for the single layer case in Figure 4.1 in that the central deflection increases with increasing internal pressure. Additional computed results for the two layer shell structure with various ply angles of the two layers are presented in Figure 4.4. Note that the first natural frequency for this case is 203 rad/s.

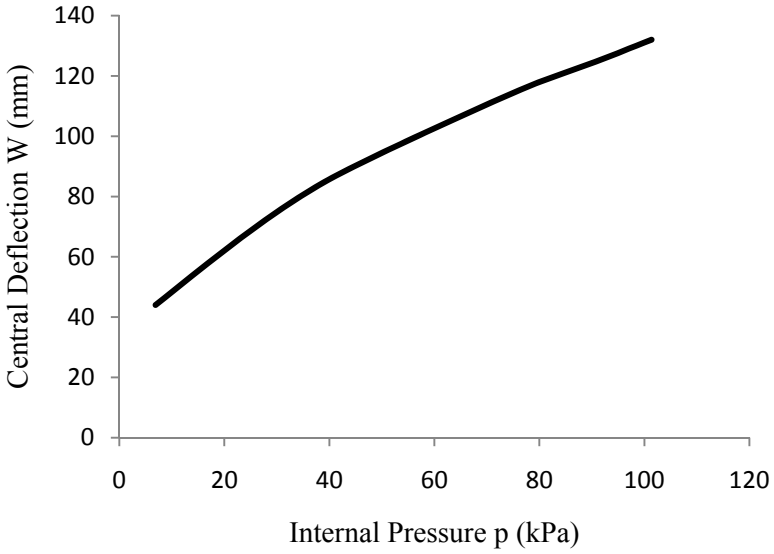

Figure 4.3 Central deflections for two layers shell [0/30].

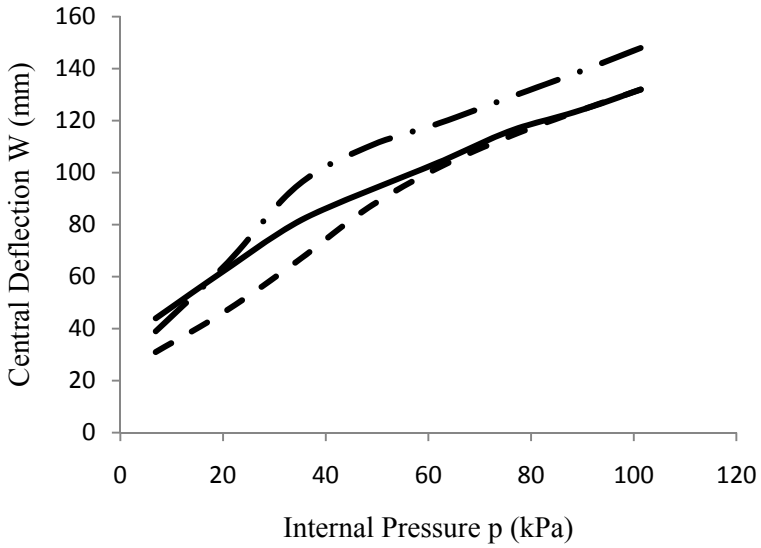

Figure 4.4 Central deflections for two layers shell with different ply angles:

– , [0/30]; –.–. , [0/60]; – – . , [0/90].

4.3.2 Bulging factors for two layers shell structure

Figure 4.5 shows the bulging factors for ply angles [0,30] with the internal pressure. The behavior is similar to that of the single layer case in that it is decreasing with increasing internal pressure. Bulging factors for the same two layers but different ply angles shell structure are presented in Figure 4.6. It can be noticed that there is not much variation between bulging factors with different ply angles.

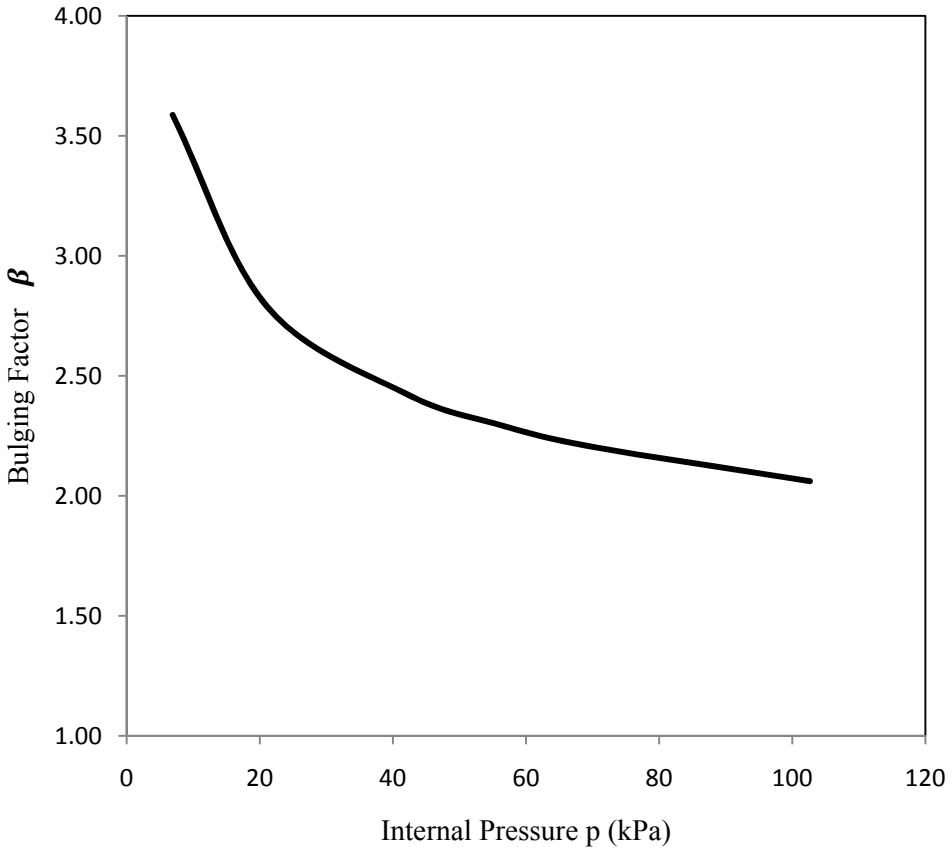

Figure 4.5 Bulging factors for two layers shell [0/30].

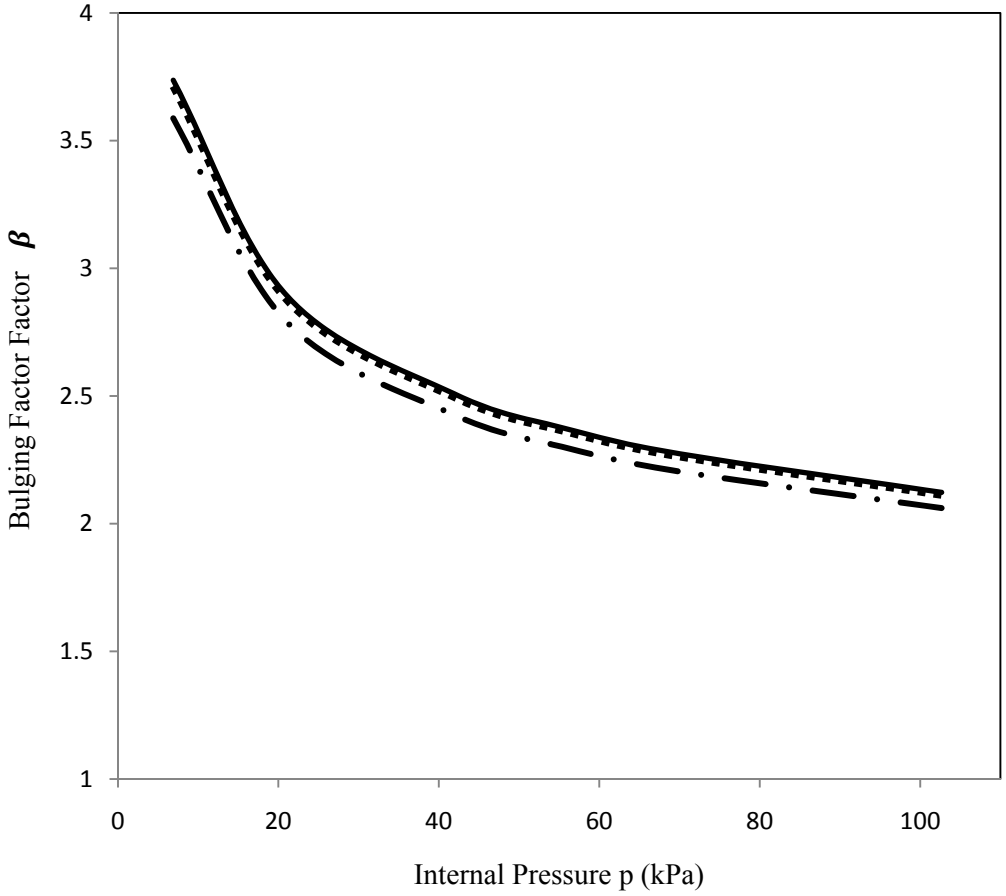

Figure 4.6 Bulging factors for two layers shell with different ply angles:

-.-. , [0/30]; - -, [0/60]; - , [0/90].

4.4 Central Deflection and Bulging Factors for Four Layers Shell Structure

Again, the total thickness of the laminated composite shell structure is the same as the single layer case. The boundary conditions are identical to those studied in previous cases. All four layers have equal thickness. The material employed is Carbon–epoxy

(AS4/3501-6) and therefore its properties are identical to those for the two layer case presented in the last section.

4.4.1 Central deflection

Figure 4.7 shows the variation of the central deflections against internal pressure, when ply angle [0/45]sym. As expected, central deflection increases with increasing internal pressure. However, central deflection accelerated within internal pressure range of 15 to 30 kPa. The first natural frequency for this case is 224.3 rad/s. Figure 4.8 shows the change in central deflections against internal pressure with ply angles being varied within the four layers. In the latter case the first natural frequency for this case is 214.3 rad/s.

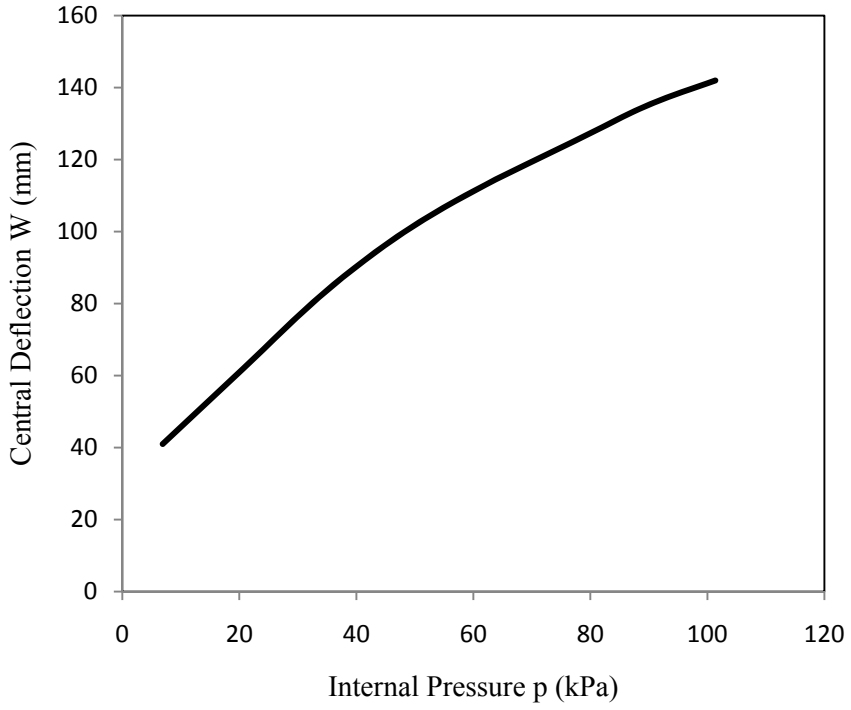

Figure 4.7 Central deflections for four layers shell $[0/45]_{sym.}$

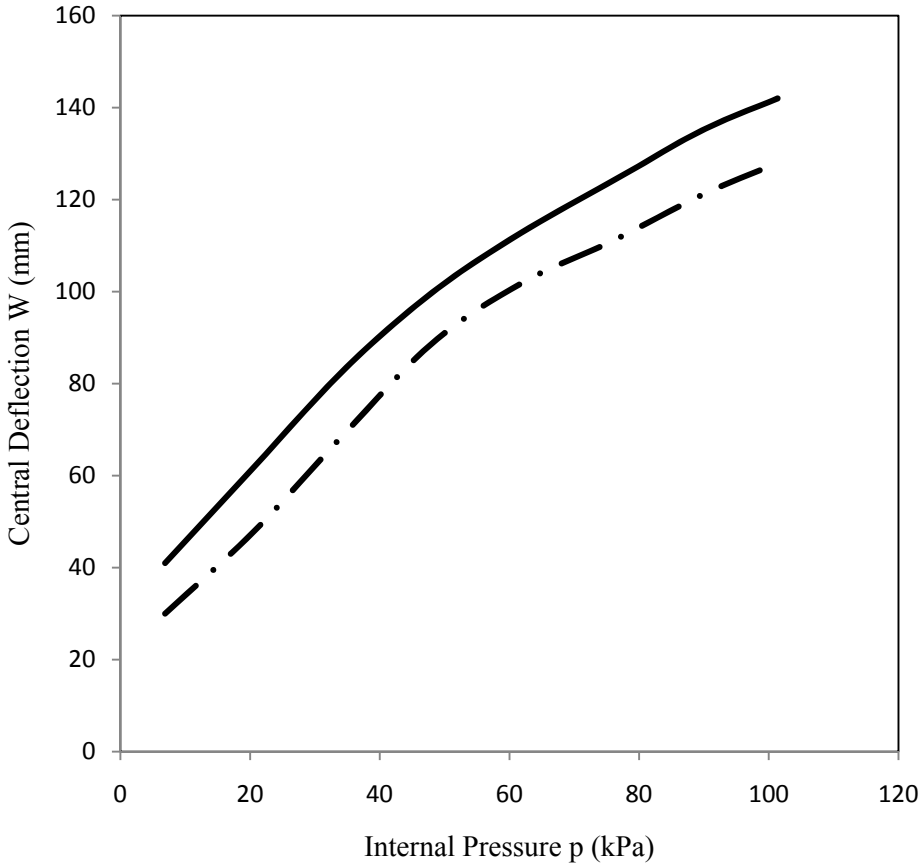

Figure 4.8 Central deflections for four layers shell with different ply angles: - , $[0/45]_{sym}$; - . - ., $[0/90]_{sym.}$

4.4.2 Bulging factors for four layers shell structure

Figure 4.9 and Figure 4.10 shows the bulging factors curve against internal pressure with fixed ply angles and varying ply angles respectively. Figure 4.9 represents the bulging factors when ply angles are kept as $[0/45]_{sym}$ for the four layers shell. It can be seen in Figure 4.10 that, change in ply angles within laminas of composite shell structure affects the bulging factors and this variation is significant.

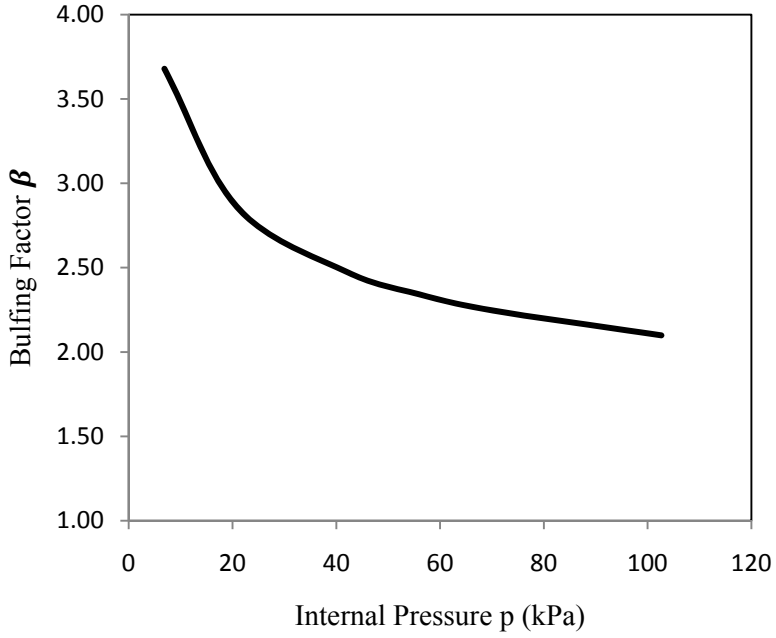

Figure 4.9 Bulging factors for four layers shell $[0/90]_{sym.}$

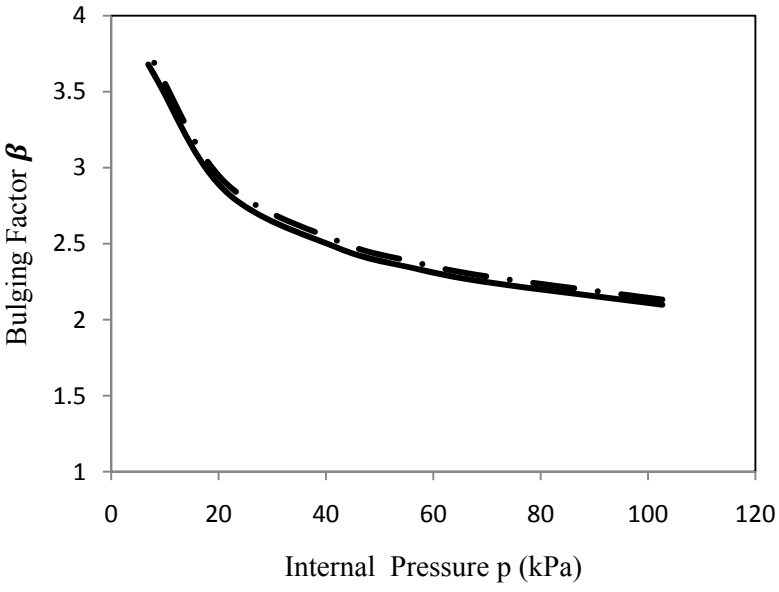

Figure 4.10 Bulging factors for four layers shell with different ply angles:

- , $[0/45]_{sym}$; -. -, , $[0/90]_{sym}$

4.5 Comparison of Bulging Factors for Shells with Different Numbers of Layers

Figure 4.11 shows the bulging factors against internal pressure. It can be noticed that, bulging factors vary with the number of layers in the laminated composite cylindrical shell structures. As shown in this figure, there is drastic reduction in the bulging factor from single layer to the two layer case.

However, very small difference in the bulging factors occurred between the two and four layers cases.

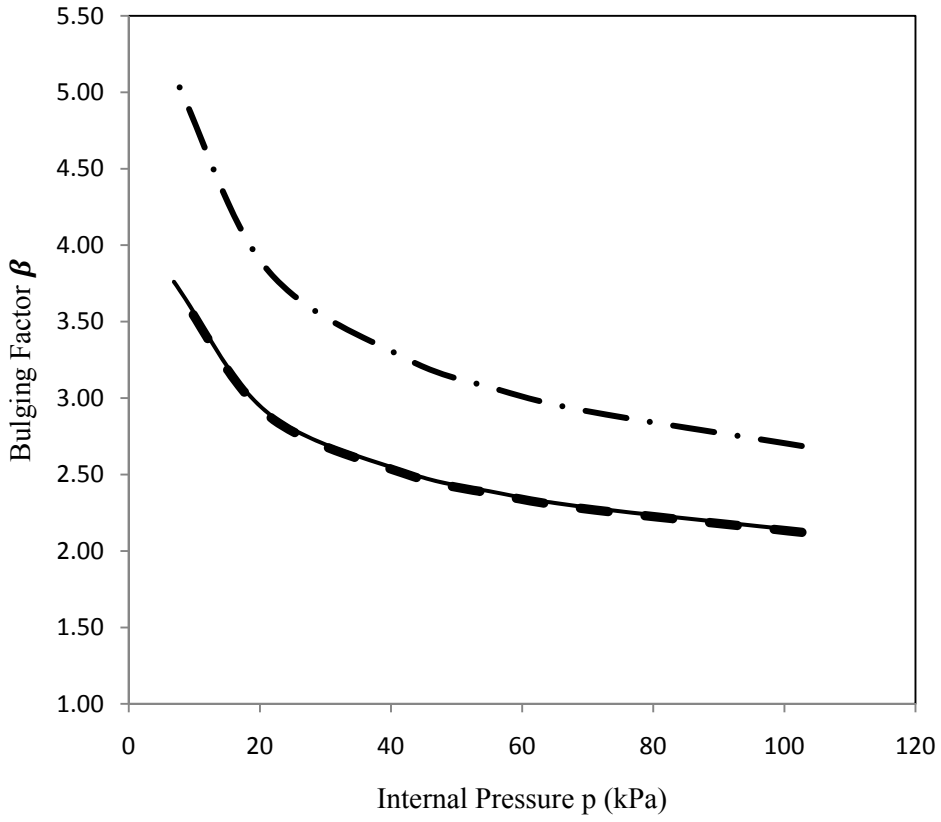

Figure 4.11 Comparison of bulging factors for different number of layers:

-.-., single layer; - -, two layers [0/90]; - , four layers $[0/90]_{sym.}$

4.6 Bulging Factors for Cracked Laminated Composite Shell Structure with Free-Free Boundary Conditions

Results discussed so far, were based on the clamped-clamped boundary conditions. In this section another set of boundary conditions is included. Aside from the boundary conditions all other geometrical and material properties are similar to those for the clamped-clamped boundary conditions cases.

4.6.1 Single layer shell structure with free-free boundary condition

Figure 4.12 show the bulging factors for the single layer cracked shell structure with free-free boundary conditions for different internal pressure. It can be clearly seen from the figure that the bulging factor reduces with increasing internal pressure. The reduction in the bulging factor is more pronounced in the range of pressure between 10 and 30 kPa while its rate of reduction is less pronounced in the range between 60 kPa and 100 kPa. It may be appropriate to note that for this case the first natural frequency for this case is 39.6 rad/s.

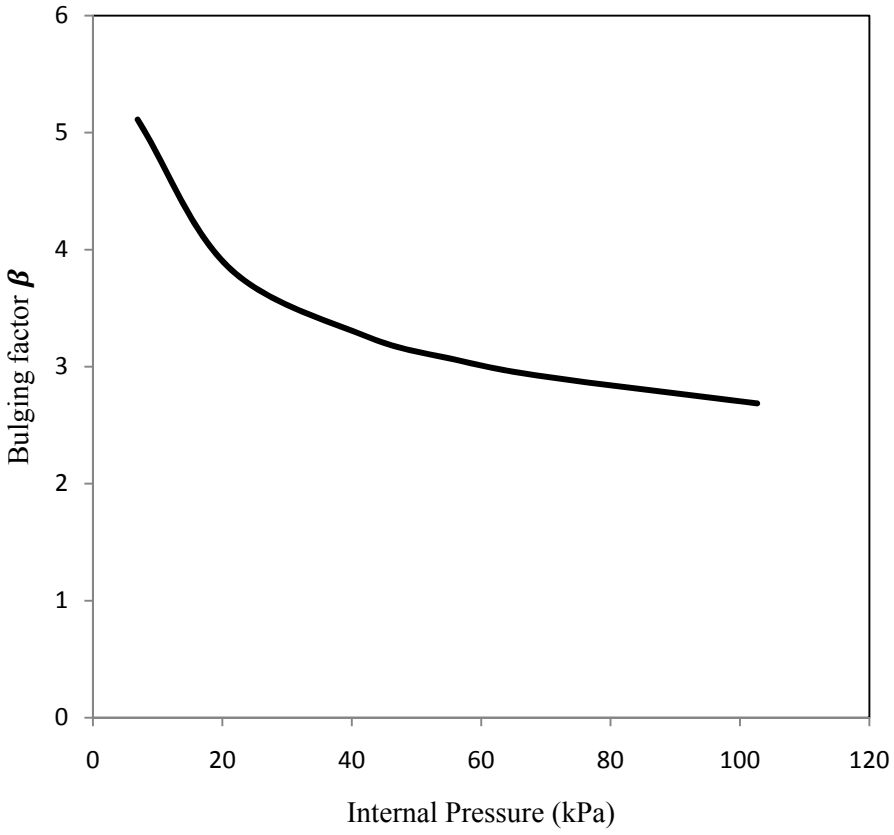

Figure 4.12 Single layer shell with free-free boundary conditions.

4.6.2 Two layers shell structure with free-free boundary conditions

Two layers cylindrical shell structure with free-free boundary conditions and different ply angles are considered in this sub-section. The computed results are presented in Figure 4.13. Note that the results for ply angles [0/90] show approximately a 10% higher bulging factor than that for those of ply angles [0/30]. Note that the first natural frequency for the case with [0/90] is 16.93 rad/s while that for the [0/30] case is 13 rad/s.

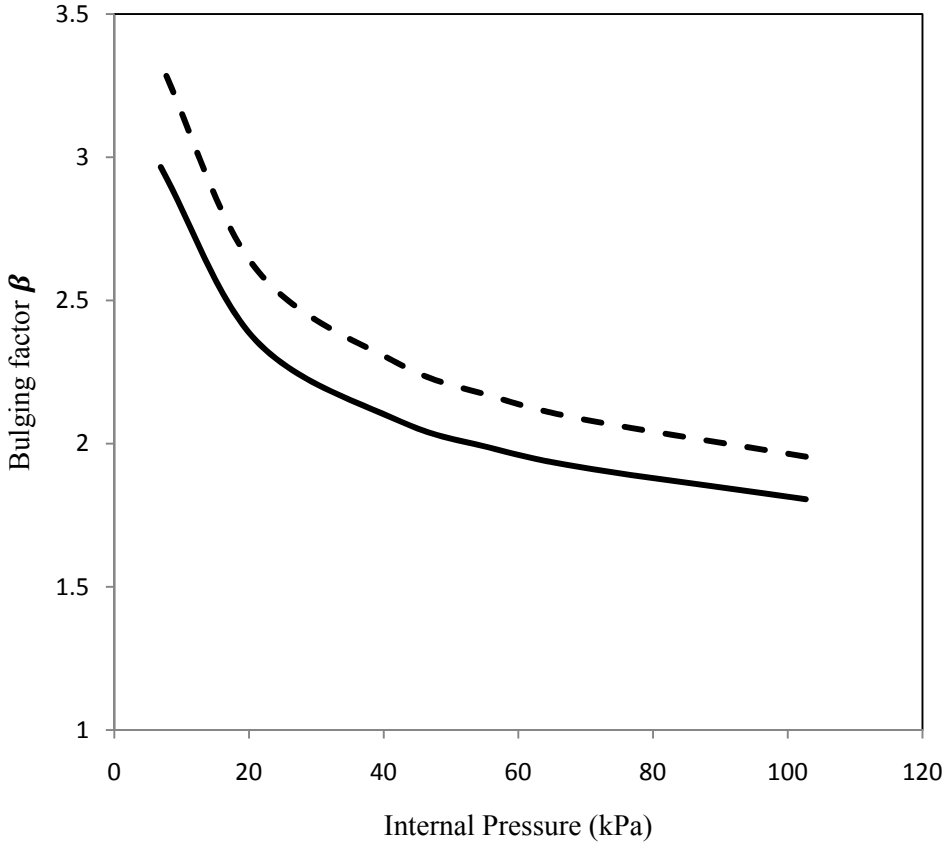

Figure 4.13 Comparison of bulging factors for two layers with free-free boundary conditions:

– , [0/30]; – – , [0/90].

4.6.3 Four layers shell structure with free-free boundary conditions

Computed results of bulging factors for the four layers shell structure are presented in Figure 4.14. Here, ply angle $[0/30]_{sym}$ and $[0/90]_{sym}$ are considered for the comparison. Both of the ply angle arrangements show reduction with the increase in internal pressure.

However, the rate of change of the bulging factor is higher within internal pressure range of 10 to 25 kPa. Results of ply angle arrangement [0/30] show a 15% reduction of the bulging factor compared with those for ply angle arrangement [0/90]. It should be mentioned that the first natural frequencies for the [0/30] and [0/90] cases are found to be 14.52 and 20.84 rad/s, respectively.

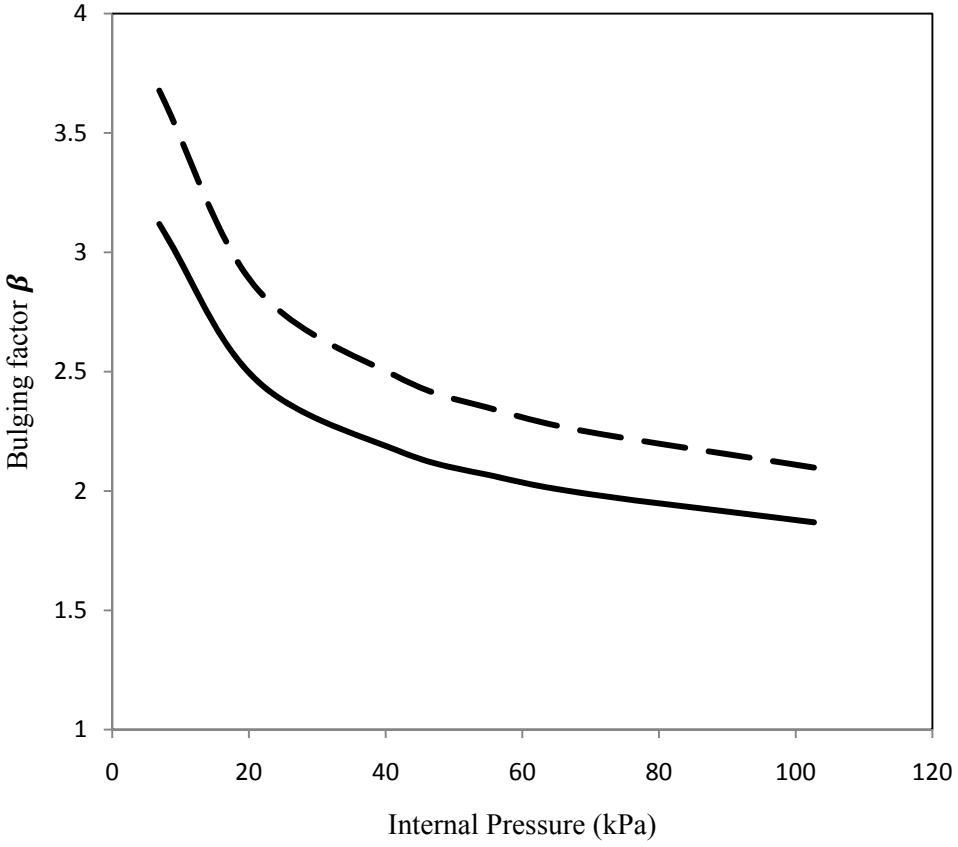

Figure 4.14 Bulging factors for four layers with free-free boundary conditions: ——, $[0/30]_{sym}$; - - -, $[0/90]_{sym.}$

4.6.4 Comparison of shell structures with free-free boundary conditions

With the bulging factors presented in the foregoing sub-sections, it is now convenient to compare all the cases in a single figure. The latter is Figure 4.15. It can be observed that average bulging factors for the two layers cases are reduced by as much as 53% compared with those for the single layers while those of the four layers cases are decreased by about 39%.

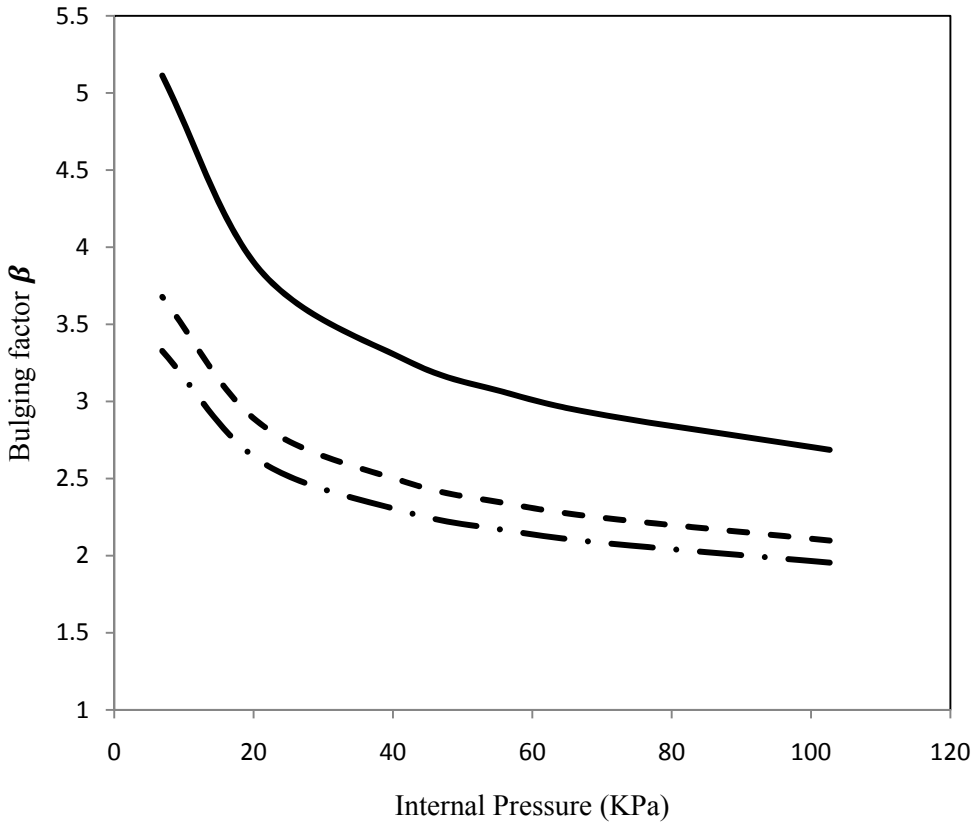

Figure 4.15 Bulging factors for different layers with free-free boundary conditions: - , single layer; -.-. , two layers [0/90]; - - , four layers $[0/90]_{sym.}$

Chapter 5 Concluding Remarks and Recommendations for Future Work

5.1 Introduction

In this chapter, summary and concluding remarks of the present research conducted are presented. Recommendations for future work are included in Section 5.3.

5.2 Summary and Concluding Remarks

In this investigation of the geometrically nonlinear responses and bulging factors of cracked laminated composite cylindrical shell structures subjected to internal pressure are studied and analyzed.

In Chapter 1, literature survey was done not only for non-cracked cylindrical laminated structures but also for deflection of cracks in pressurized shell structures. Intensive survey shows that there is very limited work reported regarding the dynamic responses and bulging factors of the cracked cylindrical shell structures. There is no work, however, on bulging factors for laminated composite shell structures although composite materials are intensively used for different parts of aircrafts. Therefore, the major focus was given to the computation of dynamic responses of central deflections of the cracks and bulging factors of laminated composite shell structures.

Chapter 2 includes the theoretical development of the approach to solving for the dynamic responses and bulging factors of laminated composite shell structures. Bulging factors for isotropic shell structures from previous work reviewed in Chapter 1 were introduced and highlighted in this chapter.

Since laminated composite materials are widely used in the aircrafts, a brief overview of composite materials and their descriptions is mentioned in this chapter. Types of composite materials are also mentioned. Advantages of different composite materials are discussed. The shell elements used in this research, hybrid strain-based laminated composite triangular shell finite elements (HLCTS) which were developed by To and Wang are briefly described and explained. These elements have several advantages such as, capability of dealing with large deformations.

Finite element models for non-cracked and cracked cylindrical shell structures are illustrated in Chapter 3. Central deflections were obtained for two layers, four layers and eight layers cylindrical composite non-cracked shell structures to study their differences. It can be also mentioned that for non-cracked shell structures not only number of laminas but also ply angles have important influence. Central deflections for the cracked shell structures are presented in the later part of this section. Cracked shell structures with single layer, two layers and four layers were studied. During the study of two layers or multilayer cracked shell structures, ply angles within laminas are varied and differences can be seen in the figures presented. It can be seen that even keeping the ply angle for the first lamina constant and changing the second ply angle also makes significant change in the central deflection.

In Chapter 4, central deflections and bulging factors for single and multilayer laminated composite shell structures when internal pressure varied are presented. For the cases with fixed-fixed boundary conditions, central deflections increase with increase in internal pressure, whereas bulging factors decrease with increasing internal pressure. It can be noticed that central deflections vary as ply angles change within the laminated composite shell structure even though the trend of central deflection increases with increasing internal pressure remains the same.

For the aforementioned cases, bulging factors reduces with increasing internal pressure. It should be noted, however, that the ply angle plays a significant role. Bulging factors for the two layers and four layers with different ply angles show little variation. Bulging factors shows 48% reduction with comparison to the two layers cylindrical shell structure, whereas, the four layers shell structure shows 55% reduction. Variation in bulging factors for two layers and four layers shows 6 to 7% reduction.

Bulging factors for cracked laminated composite cylindrical shell structures with free-free boundary conditions were obtained and discussed. As mentioned above the trend of decrease of bugling factors remains the same for free-free boundary conditions. However, in these different boundary conditions, reduction in bulging factors are 72% and 63% for two layers and four layers, respectively.

5.3 Recommendations for Future Work

First, the results of the investigation presented in the foregoing are concerned with the same crack type and size for single layer and multi layers. Therefore, bulging factors for different crack types and sizes can be examined.

Second, crack propagation can also be included in the future studies as stress intensity at cracked location is higher which may tend to propagate the crack in different direction.

Third, bulging factors for multi-cracks can be studied for laminated composite shell structures, since in practice aircrafts can have multi cracks.

Fourth, computed results presented in the foregoing obtained by applying the finite element method should be verified by experiments.

Fifth, the internal pressure applied in the present investigation can be replaced with explosive internal or external pressure to simulate internal or external explosion in or outside the aircraft.

References

[1.1] Noor, A.K., Mathers, M.D. , "Nonlinear finite element analysis of laminated composite shells," In: Oden , J.T., Becker, E.B., Craig, R.R., Dunham, R.S., Johnson, C. P., Oberkampf, W.L., *Computational Methods in Nonlinear Mechanics*, Austin, TX, 1974.

[1.2] Noor, A. K. and Hartley, S.J., "Nonlinear shell analysis of laminated shells by finite element method," *Computer and Structures*, Vol. 7.,1977, pp. 615.

[1.3] Chao, W. C., Reddy, J. N., "Analysis of laminated composite shells using a degenerated 3-D element," *International Journal of Methods in Engineering*, Vol. 20, 1984, pp. 1991-2007.

[1.4] Saigal, S., Kapania, R.K., Yang, T.Y., " Geometrically nonlinear finite element analysis of imperfect laminated shells," *Journal of Composite Materials*, Vol.20,1986, pp. 197-214.

[1.5] Swamy Naidu, N.V. and Sinha, P.K., "Nonlinear transient analysis of laminated composite shells in hydrothermal environments," *Department of Aerospace Engineering, Indian Institute of Technology*, Vol.72, 2005, pp. 280-288.

[1.6] Rothert, H., Dehmel, W., "Nonlinear analysis of isotropic orthographic and laminated plates and shells," *Computational Methods in Applied Mechanics Enigneering*, Vol. 64, 1987, pp. 429-446.

[1.7] Lin, J.J., Fafard, M., Beaulieu, D., Massicotte, B., "Nonlinear analysis of composite bridges by the finite element method." *Comput. Struct.*, Vol. 40, 1991, pp. 1151-1167.

[1.8] Madenci, E., Barut, A., "A Free-formulation-based flat shell element for nonlinear analysis of thin composite structures," *International Journal for Numerical Methods in Engineering*, Vol. 37, 1994, pp. 3825-3842.

[1.9] Zhu, J., "Application of natural approach to nonlinear analysis of sandwich and composite plates and shells," *Computational Methods of Application in Mechanics and Engineering*, Vol. 120, 1995, pp. 1031-1056.

[1.10] To, C.W.S., and Wang, B., "Transient responses of geometrically nonlinear laminated composite shell structures," *Finite Element in Analysis and Design*, Vol. 31, 1998, pp. 117-134.

[1.11] Folias, E.S., "An axial crack in a pressurized cylindrical shell," *International Journal of Fracture Mechanics*, Vol. 1, 1965, pp. 20-46.

[1.12] Folias, E.S., "On the effect of initial curvature on cracked flat sheets," *International Journal of Fracture Mechanics*, Vol. 5, No. 4, 1969, pp. 327-346.

[1.13] Copley, L.G. and Sanders, J.L. Jr., "A longitudinal crack in a cylindrical shell under internal pressure," *International Journal of Fracture Mechanics*, Vol.5, No. 2, 1969, pp. 117-131.

[1.14] Erdogan, F. and Kibler, J.J., "Cylindrical and spherical shells with cracks," *International Journal of Fracture Mechanics*, Vol. 5, No. 3, 1969, pp. 229-237.

[1.15] Rose, C. A., Young, R.D. and Starnes, J.H. Jr., "Nonlinear local bending response and bulging factors for longitudinal cracks in pressurized cylindrical shells," *American Institute of Aeronautics and Astronautics*, NASA Langley Research center, 1999.

[1.16] Ansell, H., "Bulging of cracked pressurized aircraft structure," Technical Licentiate Dissertation, *Department of Mechanical Engineering*, Linkoping Institute of Technology, Linkoping, Sweden, 1988.

[1.17] Jeong, D.Y., and Tong, P., "Nonlinear bulging factor based on r-curve data," *Proceedings of the FAA/NASA International Symposium on Advanced Structural Integrity Methods of Airframe Durability and Damage Tolerance*, Sept, 1994, pp. 327-338.

[1.18] Bakuckas, J.G., Jr., Nguyen, P.V., Bigelow, C.A. and Broek, D., "Bulging factors for reading residual strength of fuselage panels," *Presented at the International Conference on Aeronautical Fatigue*, Edinburgh, Scotland, June,1997.

[1.19] Rose, C. A., Young, R.D. and Starnes, J.H. Jr., "Nonlinear bulging factors for longitudinal and circumferential cracks in pressurized cylindrical shells subjected to combined loads," *American Institute of Aeronautics and Astronautics*, NASA Langley Research center, 1999.

[1.20] Rhaman, A., Bakuckas, J.G., Tan, P.W., Bigelow, C.A.,, "Bulging effects on longitudinal cracks in lap joints of pressurized aircraft fuselage," *Paper presented at the aging aircraft conference*, 2002, San Fransisco, Sept., pp. 16-19.

[1.21] Lazghab, T., Ayari, F., Chelbi, L., "Crack growth in cylindrical aluminum shells with inner reinforcing foam layer," *International Journal for Fracture Mechanics*, Vol. 144, 2007, pp. 159-171.

[1.22] Fu, J., "Geometrically nonlinear dynamic responses of cracked laminated composite shell structures under internal pressure," *A Thesis Presented at University of Nebraska Lincoln*, 2009.

[2.1] shttp://www.sciencedaily.com/releases/2008/04/080401110213.htm

[2.2] Daniel, I. and Ori, I., "Engineering Mechanics of Composite Materials".

[2.3] http://www.tpub.com/content/aviation/14018/css/14018_596.htm

[2.4] http://www.speedace.info/composites/carbon_fibre.htm

[2.5] Liu, M.L. and To, C.W.S., "Hybrid strain based three node flat triangular shell elements-I: Nonlinear Theory and Incremental Formulation," *Computers and Structures*, Vol. 54, No. 6, 1995, pp. 1031-1056.

[2.6] To, Cho W. S. and Wang, B., "Transient responses of geometrically nonlinear laminated composite shell structure," *Finite Element in Analysis and Design*, Vol. 31, 1998, pp. 117-134.

[2.7] Rose, Cheryl A., Young, Richard D. and Starnes Jr., James H., "Nonlinear local bending response and bulging factors for longitudinal cracks in pressurized cylindrical

shells*," AIAA/ASME/ASCE/AHS/ASC Structures, Structural Dynamics and Materials Conference 3*, St. Luice, MO, 199 pp. 1791-1800.

[2.8] Folias, E. S., "On the effect of initial curvature on cracked flat sheets." *International Journal of Fracture Mechanics*, Vol. 5, No.4, 1969, pp. 327-346.

[2.9] Erdogan, F. and Kibler, J.J., "Cylindrical and spherical shells with cracks," *International Journal of Fracture Mechanics*, Vol.5, NO.3, 1969, pp. 229-237.

[2.10] Riks, E., "Bulging Cracks in Pressurized Fuselage: A Numerical study." NLR report NLR-MP-87058*, NLR National Aerospace Mechanics*, The Netherlands, 1978.

[2.11] Chen, D and Schijve, J., "Bulging of fatigue cracks in a pressurized aircraft fuselage," *Delft Institute of Technology*, Delft, The Netherlands, LR-655,1991.

[2.12] Ansell, H., "Bulging of cracked pressurized aircraft structure," Technical Licentiate Dissertation, *Department of Mechanical Engineering*, Linkoping Institute of Technology, Linkoping, Sweden, 1988.

[2.13] Jeong, D.Y. and Tong, P., "Nonlinear bulging factor based on R-curve data," *Proceedings of the FAA/NASA International Symposium on Advanced Structural Integrity Methods for Airframe Durability and Damage Tolerance,* September, 1994, pp. 327-338.

[2.14] Bakuckas, J. G, Jr., Nguyen, P. V., Bigelow, C.A. and Broek, D., " Bulging factors for redicting residual strength of fuselage panels," Presented at the *International Conference on Aeronautical Fatigue*, Edinburgh, Scotland, June, 1997.

[2.15] To, Cho W. S., "Unpublished research notes," 2010.

[3.1] Fu, J., "Geometrically nonlinear dynamic responses of cracked laminated composite shell structures under internal pressure," *A Thesis Presented at University of Nebraska Lincoln*, 2009.

[3.2] To, C. W. S. and Wang, B., "Hybrid strain based geometrically nonlinear laminated composite triangular shell finite elements," *Finite Elements in Analysis and Design*, Vol. 33, 1999, pp. 1862-1876.

[3.3] Wu, C. Y. and Saigal, S., "Free and forced nonlinear dynamics of composite shell structures," *J. Compos. Mater*., Vol. 21, 1987, pp. 898-909.

[4.1] To, Cho W. S., "Unpublished research notes," 2010.

[4.2] Van Tooren, Michel and Krackers, Lars, "Multi-disciplinary design of aircraft fuselage structures," *Collection of Technical Papers-45th AIAA Aerospace Science Meetin*g, Vol. 14, 2007, pp. 9419-9431.

[4.3] Fu, J., "Geometrically nonlinear dynamic responses of cracked laminated composite shell structures under internal pressure," *A Thesis Presented at University of Nebraska Lincoln*, 2009.